Engineered Science
DOI: https://dx.doi.org/10.30919/es1120

Effective Machine-Learning Models for Rock Mass Deformation Modulus Estimation Based on Rock Mass Classification Systems

Mohammad Khajehzadeh,[1, 2] Suraparb Keawsawasvong[1,*] Mohammad Reza Motahari[3] and Pitthaya Jamsawang[4]

Abstract

The rock mass deformation modulus (RMDM) plays a crucial role in dam and tunnel design. This study introduces advanced machine-learning (ML) models to predict RMDM using rock mass rating (RMR) and the Q-system at the Khersan-2 dam site in southwestern Iran. Through the analysis of exploratory boreholes, the engineering geological properties of the samples, Q, RMR, RMDM, geological strength index (GSI), Hoek-Brown, and shear strength constants of the rock mass were determined. Subsequently, several effective ML models, namely random forest, multilayer perceptron backpropagation artificial neural network, Gaussian process regression, K-nearest neighbor, simple regression, and multiple linear and non-linear regression approaches, were utilized to estimate RMDM. Based on classification systems, the site was rated as having good RMR and Q categories. A new empirical relationship with high accuracy was established between Q and RMR89. Furthermore, RMDM demonstrated a strong correlation with Q and RMR, as supported by statistical analysis. The results showed the relative superiority of non-linear regression models compared to linear ones. The employed ML techniques displayed remarkable accuracy in estimating RMDM, achieving a coefficient of determination (R^2) greater than 97%. Notably, Gaussian process regression with a squared exponential kernel function stood out as the most effective approach, yielding outstanding performance in predicting RMDM with an impressive R^2=0.99 and RMSE=0.01 compared to all other investigated methods.

Keywords: Rock mass classification; Rock mass deformation; Multivariate regression, Machine-learning; Khersan-2 dam site.
Received: 14 February 2024; Revised: 13 March 2024; Accepted: 05 April 2024.
Article type: Research article.

1. Introduction

Rock mass deformation modulus (RMDM) is a crucial factor in geotechnical engineering because it directly influences the stability and deformability characteristics of rock masses. In geotechnical engineering, understanding the behavior of rock masses is essential for designing and constructing various structures, such as dams, tunnels, slopes, and underground excavations.[1,2] The RMDM represents the ability of the rock mass to deform under applied stresses and loads, and it is a fundamental parameter in assessing its mechanical response. Accurate estimation of the deformation modulus is essential for designing safe and reliable underground structures and rock engineering projects.[3]

Given the significance of the deformation modulus parameter in characterizing the mechanical behavior of rock masses subjected to loading, it finds wide application as an input in numerous finite element and boundary element numerical analyses. These analyses are instrumental in investigating the intricate distribution of stress and displacement around underground excavations, allowing engineers to gain deeper insights into the structural response and ensure the integrity and safety of such subsurface constructions.[4] Generally, this modulus parameter can be measured by dilatometry, radial loading, and plate jack test tests. In-situ tests face difficulties in implementation due to unpredictable construction conditions, high costs, operational problems, and their time-consuming nature.[5-8]

In recent years, several empirical relationships and estimation approaches have been established to forecast the RMDM. The following literature review aims to provide an

[1] *Research Unit in Sciences and Innovative Technologies for Civil Engineering Infrastructures, Department of Civil Engineering, Thammasat School of Engineering, Thammasat University, Pathumthani, 12120, Thailand.*
[2] *Department of Civil Engineering, Anar Branch, Islamic Azad University, Anar, 7741988706, Iran.*
[3] *Department of Civil Engineering, Faculty of Engineering, Arak University, Arak, 3848177584, Iran.*
[4] *Soil Engineering Research Center, Department of Civil Engineering, King Mongkut's University of Technology North Bangkok, Bangkok 10800, Thailand.*
**Email:* ksurapar@engr.tu.ac.th (S. Keawsawasvong)

overview of machine learning (ML), empirical relationships, and their applications based on a selection of relevant references. Emami Meybodi *et al.*[9] employed a machine learning-based approach to develop predictive models for estimating the RMDM. Their study focused on training the models using various input parameters, such as intact rock properties, rock mass characteristics, and geomechanical indices. The developed models demonstrated promising accuracy in predicting the RMDM. Jiao *et al.*[3] proposed an approach for predicting the RMDM. Their method considered the joint properties, including joint orientation, joint roughness, and joint persistence, and integrated them into a unified modulus estimation approach. The study showed that the multi-domain equivalent method provided reasonable estimates of the RMDM. Bellapu *et al.*[7] conducted a review and validation study on the estimation of the RMDM using the RMR system. The findings suggested that RMR can be used as a reliable indicator for estimating the RMDM, although site-specific calibration is required. Motamed-Shariati *et al*.[10] developed empirical relations for estimating the RMDM. The developed empirical relationship provided a practical approach to estimating the deformation modulus for the specific dam site. Hasanipanah *et al.*[8] proposed an intelligent prediction model for estimating the RMDM. The model considered multiple inputs of the intact and rock mass properties. The results demonstrated the effectiveness of the intelligent prediction model in estimating the deformation modulus. Aladejare *et al*.[11] highlighted the importance of intact rock properties and rock mass features to improve the accuracy of RMDM estimation. Chen *et al*.[12] assessed the influence of confining stress and performed sensitivity analyses on various variables. The analytical solution provided insights into the relationship between confining stress and RMDM. Zhang *et al*.[13] developed a new estimation method for RMDM prediction considering anisotropy. They introduced an anisotropy index to quantify the influence of joint orientations on the deformation modulus. The proposed method provided a more comprehensive approach to estimating the deformation modulus for jointed rocks. Polemis Júnior *et al*.[14] conducted a study for estimating the RMDM using 48 different rock masses. They evaluated the performance of several established empirical relationships and identified their strengths and limitations. The study provided insights into the accuracy and applicability of different methods under various rock mass conditions. Hua *et al.*[15] proposed RMDM estimation models based on in-situ tests. Their study involved comprehensive field investigations and a large dataset of deformation modulus measurements. They developed empirical models considering key parameters such as intact rock properties, discontinuity characteristics, and rock mass quality. The models demonstrated good accuracy in predicting the RMDM based on in-situ tests. Que *et al.*[16] analyzed the behavior of columnar jointed specimens under different loading conditions and proposed a new equation to estimate the RMDM. Koopialipoor *et al.*[17] proposed the use of stacking machine learning approaches for predicting rock deformation. Other researchers have conducted a comparative study with the help of statistical methods, multivariate regression, and multilayer perceptron back propagation artificial neural network (MLPBPANN) to predict RMDM.[18,19] Tokgozoglu *et al.*[20] investigated the effect of overburden stress on the deformation modulus of rock mass using MLPBPANN models. They developed two models considering the overburden stress and two other models without considering the overburden stress parameter. They stated that models without overburden stress are less accurate than models containing overburden stress. Nejati *et al.*[21] and Chun *et al.*[22] have also used the RMR classification system to predict the RMDM. Barami and Bania[23] conducted a comprehensive study on the effect of effective factors on the equivalent deformation modulus based on analytical and experimental formulas. In addition, the effects of various parameters, such as the ratio of gallery dimensions to the dimension of the loading plane, in situ stresses, and stress ratio were considered. The results showed that when the ratio of the dimensions of the gallery to the dimension of the loading plate was greater than 10, the effect of the dimension of the gallery disappeared. An increase in the stress ratio and maximum horizontal stress at constant depth led to an increase in the RMDM.[23] In an empirical study, a functional equation for estimating RMDM using point load and rock quality designation (RQD) was presented, and the statistical evaluation of the proposed average displayed that RMDM can be reliably predicted by the developed equation.[24] Comparison of in-situ modulus values with values generated from eight experimental relationships showed that the actual values and the forecasted values are equal where the rock is intact, but the values are significantly different where the rock is weathered.[25] Panthee *et al.*[26] studied the effect of Q and RMR on the RMDM of different rock types at the site of the Kulekhani III hydropower project using regression analysis. Radovanović *et al.*[27] evaluated multivariate linear regression (MVLR) and MLPBPANN models to estimate the RMDM using shear and compressional wave velocities in the rock mass at the Iron Gate 1 dam site on the Danube River. The results showed that the model based on MLPBPANN performed better compared to MVLR. Noorian *et al.*[28] used two-dimensional numerical methods and finite element models to define the resistance and deformability of the rock mass. Sari[29] with the help of stochastic modeling techniques to quantify rock mass engineering parameters such as the modulus of deformation in pyroclastic rocks, has tried to estimate the RMDM. Table 1 summarizes the expressions and methods previously used in the literature by several of the aforementioned works.

According to the suggestions of previous researchers, each relationship is applicable to a particular area and a range of values.[7,8] Therefore, depending on the type and importance of the project or in the initial stages of studies of important projects, it is economical to estimate the RMDM by indirect

methods using geotechnical parameters of the rock mass. Although previous studies have used various properties for indirect estimation of deformation modulus, none of these studies have used the comprehensive properties of rock mass and intact rock included in Q and RMR classification systems. On the other hand, the methods presented for each region can be generalized to some extent and local empirical relations should be developed for each region. Also, in previous studies, several different methods have been rarely used to estimate the RMDM.

The most significant innovation of this research lies in the ability to develop an optimal and ideal model for estimating the costly parameter of rock mass deformation modulus using statistical and intelligent methods, based on the results of low-cost tests such as rock mass classification systems. This approach eliminates, the laborious and time-consuming inside borehole tests, such as the dilatometry test.

The main contributions of this article can be summarized as follows:

1 The geo-mechanical properties of the Khersan-2 dam site (including the properties of rock and stone material) are investigated and evaluated.
2 The RMDM is estimated based on dilatometry test results and rock mass classification systems using statistical and intelligent methods.
3 The effectiveness of six different ML models to estimate the RMDM has been investigated and the best model is introduced.
4 Empirical relationships are presented to estimate the deformation modulus and rock mass rating (RMR) classification system.
5 Relationships of previous researchers to estimate RMDM and RMR classification systems are evaluated and their accuracy is determined.

Table 1. A summary of empirical relationships to estimate RMDM.

Reference	RMDM estimation method	Developed equation	Eq. No.
Emami Meybodi et al.[9]	Machine learning-based predictive models	-	(1)
Jiao *et al* [3]	Multi-domain equivalent method	-	(2)
Bellapu *et al*.[7]	Estimation based on Rock Mass Rating	$RMDM = 0.00011RMR^3 - 0.0088RMR^2 + 0.2RMR - 1.3$	(3)
Motamed-Shariati *et al*.[10]	Empirical relations for a specific dam site	RMDM = 35.16 *Ln(RMR)-131.59	(4)
Hasanipanah *et al.* [8]	Cascaded forward neural network models	-	(5)
Aladejare *et al*.[11]	Evaluating previous relationships	-	(6)
Chen *et al.*[12]	Analytical solution considering confining stress	-	(7)
Zhang *et al.*[13]	Deformability assessment of Jointed rock masses	-	(8)
Polemis Júnior *et al.*[14]	Comparative study of empirical methods	-	(9)
Hua *et al.* [15]	Estimation models based on in-situ tests	RMDM = 1.42Q +3.42	(10)
Que *et al*.[16]	Estimation based on physical model tests	-	(11)
Chun *et al.*[22]	Estimation based on various functions	$RMDM= 1.3326\ e^{(0.0364RMR)}$	(12)
Ching *et al.*[30]	Quasi-site-specific prediction	-	(13)
Fattahi and Moradi, [31]	RMDM prediction using statistical methods	$RMDM=2.87e^{0.094RQD}$	(14)
Khabbazi *et al.*[32]	Study of empirical methods	$RMDM = 9*10^{-7}RMR^{3.868}$	(15)
Nejati *et al.*[21]	Study of empirical methods	RMDM = 0.163RMR - 5.17	(16)
Kavur *et al.*[33]	Estimation based on various functions	$RMDM = 4^{(RMR-20)/20}$	(17)
Alemdag *et al.*[18]	RMDM prediction using statistical methods	$RMDM =0.058e^{0.0.0785RMR}$	(18)
Kıncal and Koca [34]	RMDM prediction using statistical methods	$RMDM = 0.0237 \times e^{(0.0975 \times RMR)}$,	(19)
Akram *et al.*[35]	Study of empirical methods	RMDM = 1.73 Q+7.07	(20)
Palmström and Singh[36]	Study of empirical methods	$RMDM = 8\ Q^{0.4}$	(21)
Shen *et al.*[37]	RMDM prediction using statistical methods	$RMDM = \mathbf{110\ e^{[-(RMR-110)/37)2]}}$	(22)
Fattahi and Moradi [31]	Use of the RMR system to predict of RMDM	$RMDM = \mathbf{9}\times\ \mathbf{10^{-6}}*RMR^{3.4}$	(23)
Hussain *et al.*[38]	RMDM prediction using statistical methods	$RMDM = 1.56RMR+0.04I_{S50}-75.25$	(24)
Motamed-Shariati *et al.*[10]	Study of empirical methods	$RMDM= 1.64*Q^{\wedge 0.8}$	(25)
Read *et al.*[40]	RMDM prediction using statistical methods	$RMDM = 0.1\ (RMR\ /10)^3$	(26)
Kang *et al.*[39]	Estimation based on various functions	$RMDM = \mathbf{10^{((RMR-16)/50)}}$	(27)
Bieniawski[41]	RMDM prediction using statistical methods	RMDM =−2RMR 100, For RMR> 50	(28)
Serafim and pereira[42]	Study of empirical methods	RMDM =10(RMR−10)/40, For RMR < 50	(29)

In the above equations, RMDM represents the estimated deformation modulus, Q is the Q-value, RMR is the rock mass rating, IS50 is the point load index.

2. Research methodology

2.1 Study area features

The concrete dam of Khersan-2 is located approximately 60 kilometers southwest of the city of Lordegan in Chaharmahal-Bakhtiari province. The site of Khersan-2 dam is located at coordinates 31.25 °N and 50.36 °E in the Zagros Mountains, west of Iran. Fig. 1 presents the depositional features of the Khersan-2 dam site.

The Khersan-2 dam site exhibits stratigraphy comprising three distinct stratified formations, arranged from bottom to top. These formations include Asmari, Gachsaran, Aghajari, and Quaternary deposits. With the exception of the surface power plant, the majority of the dam site's structures are situated within the upper Asmari formation (AF). This formation is characterized by thick to medium-layered limestones displaying regular layering, with a minor presence of thin-layered limestones transitioning to marl limestones.[43]

2.2 The RMR classification

The RMR classification was presented by Bieniawski,[41] and this classification was modified in 1989.[4] RMR takes into account five main parameters: rock strength, rock quality, joint spacing, joint condition, and groundwater situations. The RMR system assigns a numerical value to each of these parameters based on site observations and measurements. The individual scores are then combined to calculate the overall RMR value, which ranges from 0 to 100. A higher RMR value indicates a more favorable rock mass condition, implying better stability and engineering properties. If, in the calculation of the RMR value, the score of the underground water is ignored (in dry situations) and the orientation of the joints is not considered, the calculated RMR is called RMR89. At the Khersan-2 dam site, RMR89 values have been determined in five-meter sections of 19 exploratory boreholes. Fig. 2 displays some of the boreholes along the dam axis.

2.3 Q classification system

To calculate Q values, the score of each of the parameters of the Q classification system[44] for every five meters of each borehole was determined using tables and charts (Eq. 30). Rock quality designation (RQD) was also determined using cores obtained from drilling cores.

$$Q = \frac{RQD}{J_n} * \frac{J_r}{J_a} * \frac{J_w}{SRF} \quad (30)$$

In this equation, Jr and Jw represent the score of the joint roughness and the score of the amount of water in the joints, respectively. Jn and Ja are the scores of the number of joint sets and the weathering of the joint surfaces, respectively. The state of active stresses in the rock mass is also expressed by SRF (stress reduction factor). RQD is also determined by dividing the total length of cores equal to or greater than 10 cm by the length of the drilling run. The rock mass classification methods are presented in Table 2.

Table 2. Category of rock mass using the Q[44] and RMR[4]

Q	Rock mass category	RMR	Rock mass category
0.10-1.00	Very Weak	<20	Very weak
1-4	Weak	40-21	Weak
4-10	Medium	60-41	Fairly good
10-40	Good	80-61	Good
40-100	Very good	100-81	Very good
100-400	Excellent		

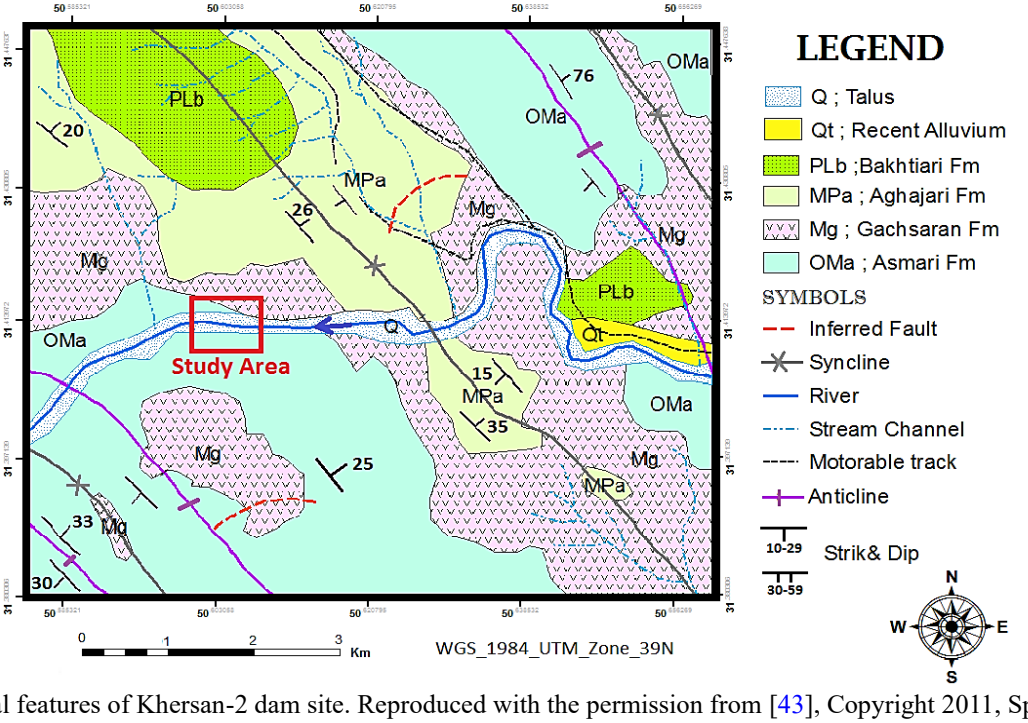

Fig. 1 Depositional features of Khersan-2 dam site. Reproduced with the permission from [43], Copyright 2011, Springer Science Business Media B.V.

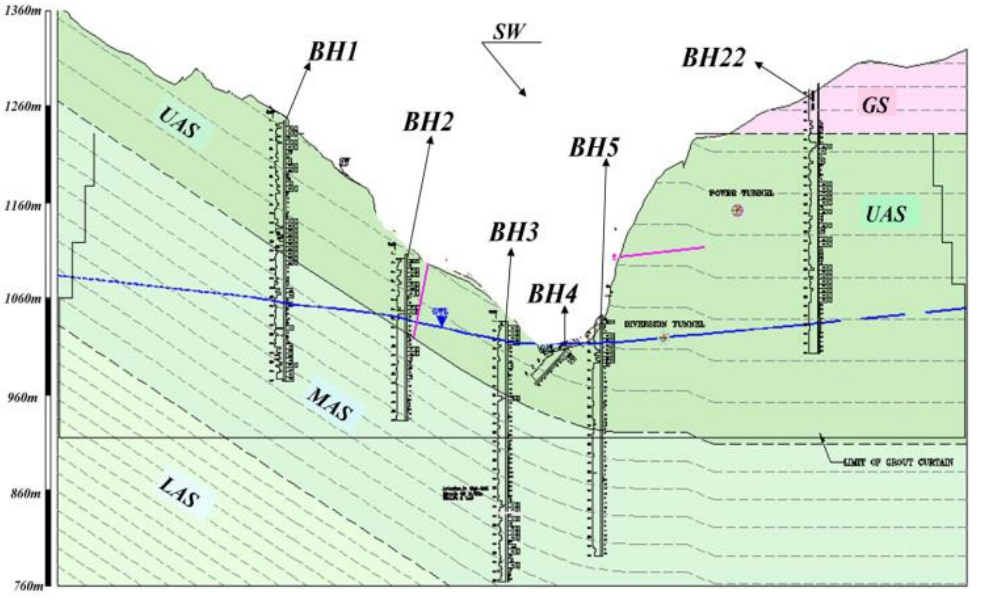

Fig. 2 Location of some of the boreholes at the dam axis.

2.4 Dilatometer test and Hoek-Brown's parameters

To measure the RMDM, a flexible dilatometer and volume change analysis were employed. In this way, in boreholes with a diameter of 101 mm and a predetermined depth, the dilatometer is sent in the form of a metal cylinder with a rubber cover, then by introducing compressed air into the space between the middle part of the metal and the rubber cover, to the wall of the borehole. Pressure is applied with maximum values of 3, 7, and 10 MPa in a stepwise manner, and the deformation modulus of the borehole wall is recorded in each step.

To calculate the rock mass shear strength parameters using the Hoek-Brown method,[45] experimental outcomes and rock mass classification were used. Equations 31-34 were used to calculate Hoek-Brown's constants.[45]

$$\sigma_1' = \sigma_3' + \sigma_{ci}\left(m_b \frac{\sigma_3'}{\sigma_{ci}} + s\right)^a \quad (31)$$

$$S = \mathrm{Exp}\left(\frac{GSI-100}{9-3D}\right) \quad (32)$$

$$a = 0.50 + \frac{1}{6}\left(e^{(-GSI/15)} - e^{(-20/3)}\right) \quad (33)$$

$$m_b = m_i \mathrm{Exp}\left(\frac{GSI-100}{28-14D}\right) \quad (34)$$

2.5 Gaussian process regression (GPR)

A Gaussian process (GP) is a set of random variables that exhibit the property of being distributed according to a Gaussian distribution. GPR is a method used to classify data by leveraging the underlying structures present within it. In a GP, there is a distribution function referred to as "*f*," which is defined as a mapping from the input space "*X*" to the real space "R." For any finite subset of "*X*," the marginal distribution of "$f(x_1), f(x_2),\ldots,f(x_n)$" conforms to a multiple normal distribution.[46,47] The parametric Gaussian process is defined as follows using the $m(x)$ mean function and the $k(x_i, x_j)$ covariance function.

$$f|X \sim N(m(x), K(X,X| \quad (35)$$

The equivalent relation of Eq. 35 is:

$$f(x) \sim gp\ (m(x), k(x_i, x_j)) \quad (36)$$

In the above relationship, the X matrix rows are input vectors, f is a vector of functions, and $K(X, X)$ denotes the $n \times n$ covariance matrix so that $Kij = k(xi, xj)$.

In order to initialize the GP, the regression model of the Gaussian process, considering y as an observation along with the Gaussian error ε, is expressed as Eq. 37[47]

$$y = f\ (x) + \varepsilon, e \sim N\ (0, \sigma_n{}^2) \quad (37)$$

The common distribution of y training outputs and f_* test outputs with zero average function are shown in the following equation (Eq. 38):

$$\begin{bmatrix} y \\ f_* \end{bmatrix} \sim N(0, \begin{bmatrix} K\ (X,X) + \sigma_n^2 I & K\ (X, X_*) \\ K\ (X_*, X) & K\ (X_*, X_*) \end{bmatrix}) \quad (38)$$

where X^* and X are the test and training data matrix of the model, respectively. By binding f_* on the y observation, the prediction of the distribution can be displayed as follows (Eq. 39):

$$f_* \left| X, y, X_* \sim N(\bar{f}_*, V\ (f_*)) \right| \quad (39)$$

where, $\bar{f}_*$ and $V(f_*)$ are obtained from Eqs. 40 and 41.

$$\bar{f}_* = K\ (X_*, X)\ [K(X,X) + \sigma_n^2 I]^{-1} y \quad (40)$$

$$V\ (f_*) = K\ (X_*, X_*) - K\ (X_*, X)[K(X,X) + \sigma_n^2 I]^{-1} K(X, X_*) \quad (41)$$

For the covariance matrices, the symbols $K\ (X_*, X_*)$, $K\ (X_*, X)$ are similar to the former $K(X, X)$ symbol. Based on Eq. 39, the forecast mean is calculated by combining the observed values of y using a linear approach. The coding of GPR relies on the assumption that inputs that are in close proximity are likely to yield similar outputs. As a result, higher weights are assigned to samples with similar values.

2.6 The MLPBPANN

The MLPBPANN generally refers to the combination of a multilayer perceptron (MLP) architecture with the

backpropagation (BP) learning algorithm to train an ANN. The MLP architecture involves multiple layers of solid nodes, where information flows in a feedforward manner from the input layer to the output layer.[48,8] The process of BP involves modifying the weights within a network by utilizing the computed error, aiming to reduce the disparity between the anticipated output and the intended output. By combining the MLP architecture and the BP algorithm, MLPBPANN enables the training of artificial neural networks to learn and make predictions or classifications based on input data.[8] The basic operation of an ANN involves propagating input data through the network, with each neuron applying an activation function to the weighted sum of its inputs. This process generates output values that are used as inputs for the next layer until the final output is obtained.[8,49] During the training phase, an ANN adjusts its weights and biases by iteratively processing training examples and comparing the forecasted results with the real results. This process is typically done using optimization algorithms like BP.[50]

2.7 Random Forest (RF)

The main idea behind RF is to combine the predictions of multiple decision trees to make more accurate and robust predictions. Each decision tree in the forest is trained on a randomly selected subset of the training data and uses a random subset of features for splitting at each node. This randomness helps to decorrelate the individual trees and reduces overfitting.[17,38] RF is resistant to overfitting due to the randomness introduced by using bootstrap samples and random subsets of features.Here's a general overview of how RF approach.[17,38]1 Random subset creation: bootstrap samples by randomly selecting subsets from the original training data with replacement. These subsets, also known as "bootstrap samples," are used to train the individual decision trees in the RF ensemble.2 Decision tree training: A decision tree is trained for each bootstrap instance using a random subset of features at each node. The decision tree is grown by recursively dividing the data via the selected features and their optimal splitting criteria.3 Ensemble prediction: After completing the training process for all the decision trees, predictions are made by each tree on the test data. The average of the predictions from all trees is used as the final forecast. In the current research, RF modeling was done using R statistical software. To obtain the number of designated variables in each tree and nods of trees, the 10-fold cross-validation process has been used.

2.8 The KNN method

This approach identifies the class of new data by averaging its k nearest neighbors during the training phase, using a distance metric. For this purpose, Euclidean distance was used in this research. The key steps involve loading training data, computing distances to all data, choosing the K nearest neighbors, and forecasting the new values.[47] Cautious choices regarding k, the distance metric, and handling unnecessary datasets are critical. With large datasets, KNN can perform more accurately. KNN serves as a simple and valuable benchmark for generating complex ML models.[47] Like other methods, 75% of the data was allocated for training the model and 25% of the data was used to test the constructed KNN model.

2.9 Normalizing data and model evaluation

Normalizing variables is a crucial step in ML, typically achieved by scaling values between -1 and 1, as outlined in Eq. 42. This process is essential for improving the efficiency of gradient descent and mitigating the impact of extreme input values on weight.

$$X_{\mathrm{nv}}=2\left(\frac{X_a-X_{min.}}{Xmin._{max.}}\right)-1 \quad (42)$$

X_{nv} represents the normalized value of the X parameter, X_a is the actual value of X, X_{min} and X_{max} denote the minimum and maximum values of X parameter, respectively.

To evaluate method efficiency, key metrics including the performance index (PI), mean absolute percentage error (MAPE), root mean square error (RMSE), variance accounted for (VAF), and determination coefficient (R^2) were employed. These metrics, widely utilized by researchers serve as valuable tools for model evaluation.[31,47,51]

3. Results and discussions

Empirical relationships and intelligent models are two indirect methods of estimating rock engineering properties at the project site. In recent years, researchers have drawn attention to providing models and relationships to estimate rock properties based on laboratory and in-situ tests.[9,18] Indirect approaches become more significant when the rocks are weak (such as marl, marl limestone, gypsum, and anhydrite investigated in this research), and jointed, and sampling is problematic, especially in deep drilling. Collecting standard specimens for destructive experiments (such as compressive strength tests) and conducting in-situ tests such as dilatometry on these types of rocks takes a lot of time and money.[19,52,17]

In this section, after presenting and comparing the results of laboratory and in-situ tests with the existing standards and the classification of intact rock and rock mass at the studied site, some experimental relationships and models for estimating the RMR classification system and the deformation modulus are presented.

3.1 Intact rock engineering properties

The engineering characteristics of the site's rock samples under both saturated and dry conditions are displayed in Table 3. According to Anon's[53] classification, both dry and saturated limestone specimens fall into the very high category based on the average compressional wave velocity (Vp). Meanwhile, limestone marl and marl limestone specimens were categorized as low classes. The findings indicate an increase in Vp and shear wave velocity (Vs) due to the sample saturation. Using density, Vp, and Vs, the dynamic elastic modulus (Ed) and dynamic Poisson ratio (DPR) were calculated and presented in Table 3. Notably, highly porous

samples exhibit a broad spectrum of Vp and Vs when saturated.[50] Also, Table 3 presents the physical characteristics, such as density, water absorption (Wa), and porosity (n) of borehole-derived specimens. The lithological composition, encompassing limestone, marl limestone, calcareous marl, and marl, is described by varying colors and textures. Limestone appears creamy and light gray to brownish gray, while marl limestones and calcareous marls exhibit gray to greenish gray color, especially in the middle Asmari formation. Distinguishing these rocks in hand samples is challenging, but calcareous marl shows lower strength and a relatively lighter color. Marl is characterized by a fine texture and gray to brown color. Porosity classification places calcareous samples in the lower class, marl limestone and calcareous marl specimens in the high category, and anhydrite and gypsum specimens were categorized in the very high category.

The objective of the UCS test was to ascertain the uniaxial compressive strength (UCS), static elastic modulus (Es), and static Poisson's ratio (SPR) of rock samples from the dam site under both dry and saturated situations. The factors influencing rock UCS are broadly categorized into internal and external factors. Internal factors are intrinsic rock characteristics, including mineral types, porosity, density, grain size and shape, void ratio, and anisotropy.[54-56] External factors, on the other hand, depend on test-related aspects such as method, device, environmental conditions, and the operator. These encompass specimen size, shape, height-to-diameter ratio, friction between loading plates and specimens, loading rate, sample connection to the test machine, sample moisture, and composition of liquids.[50] Table 3 presents the UCS, Es, and Poisson's ratio for each rock type at the dam site. Dry limestone samples exhibit high strength, whereas saturated limestone samples fall into the medium strength class. Marl limestone and both dry and saturated limestone marl specimens are categorized as medium and low strength, respectively. Anhydrite and dry gypsum were classified in a very low resistance category.[53] Saturation leads to decreased static properties and increased Poisson's ratio, a phenomenon reported by other researchers.[50] Lithology, water absorption, porosity, mineral type and amount, and cement type and amount influence sample resistance in dry and saturated conditions.[57-59] Vasarhelyi[60] stated that saturated sandstone UCS in the UK is approximately 75.6% of dry UCS, with tangential and secant modulus in the saturated condition at 76.10% and 79.00% of dry states, respectively. The type and quantity of clay minerals significantly affect the strength of foundation materials.[61,62] Clay minerals reduce the strength of the sample by absorbing water.[63] These minerals can lead to low shear resistance, swelling, soil dispersive, and settlement of the foundation of the structure.[61] When studying the stability of the dam site, it is very important to pay attention to the karstification potential of limestone and the type of clay minerals in marl rocks.[64] Due to the existence of limestone and gypsum lithologies at the dam site, the possibility of risks related to karstification in the site should be considered. Also, due to the presence of clay minerals in marl rocks, risks such as swelling and settlement of dam site should be considered.

3.2 Rock mass properties of the dam site

Dilatometry tests, determination of rock mass quality index (RQD), checking the condition of discontinuities, distance of discontinuities, and checking the condition of underground

Table 3. The mean of engineering characteristics of the site's intact rock samples.

Conditions	Lithology	UCS (MPa)	Es (GPa)	SPR	Vp (m/s)	Vs (m/s)	Ed (GPa)	DPR	Wa %	n %	Density (g/cm^3)
Dry	Yellow limestone	111.09	37.2	0.29	5022	2900	53.7	0.25	1.88	4.78	2.53
	Gray limestone	121.16	37.34	0.24	4934	2978	56.62	0.24	1.12	2.93	2.58
	Marl limestone	70.88	21.31	0.21	3450	2081	24.45	0.22	3.54	8.88	2.49
	Gypsum and anhydrite	26.75	8.56	0.2	3100	2001	18.2	0.2	10.61	22.06	2.08
Sat.	Yellow limestone	88.54	29.8	0.32	5145	3025	60.26	0.25	-	-	2.59
	Gray limestone	85.48	26.92	0.26	5081	3068	60.4	0.23	-	-	2.63
	Marl limestone	44.94	14.93	0.22	-	-	-	-	-	-	2.56
	Gypsum and anhydrite	17.9	5.64	0.21	-	-	-	-	-	-	2.3

water were conducted to determine the RMDM using Q and RMR at exploratory boreholes of the dam site. In this study, the RMDM of the Khersan-2 dam site was approximated using 88 data points from dilatometry test results and rock mass geo-mechanical characteristics. Table 4 displays the values of the geo-mechanical parameters at the dam site. The site rock mass falls into the good, fairly good, and medium categories based on the Q and RMR. Two examples of core boxes are presented

Table 4. The values of the geo-mechanical parameters at the dam site.

Sample	Depth (m)		RMR89	Q	RMDM	Sample	Depth (m)		RMR89	Q	RMDM
	From	To			(GPa)		From	To			(GPa)
S1	2.3	75.05	65	6.00	19.45	S45	38.66	52.1	52	3.00	11.92
S2	75.05	82.9	64	8.00	22.58	S46	52.1	130.1	69	19.00	31.96
S3	82.9	100.05	67	11.00	26.03	S47	130.1	250.05	74	24.00	34.50
S4	100.05	112.4	67	10.00	25.00	S48	250.05	260	63	8.00	22.57
S5	112.4	115.05	64	15.00	29.40	S49	1.94	11.4	63	8.00	22.57
S6	115.05	120.9	65	14.00	28.65	S50	11.4	22.2	72	16.00	30.10
S7	120.9	125.45	63	16.00	30.10	S51	22.2	250	69	18.00	31.38
S8	125.45	129.4	64	15.00	29.40	S52	0.7	16.8	58	5.00	17.47
S9	129.4	133.65	70	20.00	32.52	S53	16.8	35	57	4.20	15.58
S10	133.65	141.7	63	15.00	29.40	S54	35	50	63	8.00	22.57
S11	141.7	152.25	67	13.00	27.84	S55	17	60	67	13.00	27.84
S12	152.25	168	66	11.00	26.03	S56	4.7	10	57	4.00	15.05
S13	168	172.45	61	7.00	21.12	S57	10	70	60	6.00	19.45
S14	172.45	180.1	64	11.00	26.03	S58	2	8.7	60	6.00	19.45
S15	180.1	190	42	1.50	4.40	S59	8.7	280	67	13.00	27.84
S16	190	200.1	45	2.00	7.52	S60	2.7	12	42	1.00	22.00
S17	200.1	204.1	63	8.60	23.36	S61	14.3	25	61	7.00	21.12
S18	204.1	210.1	69	16.00	30.10	S62	25	35	58	5.00	17.47
S19	210.1	221.95	69	16.00	30.10	S63	35	43.7	63	8.00	22.57
S20	221.95	223.4	46	1.80	6.38	S64	43.7	55	58	5.00	17.47
S21	223.4	230	69	19.00	31.96	S65	55	62.15	48	2.00	7.52
S22	230.6	237.8	71	20.00	32.52	S66	62.15	75	65	10.00	25.00
S23	237.8	243.1	71	20.00	32.52	S67	1	6.8	64	9.00	23.85
S24	243.1	280	57	5.00	17.47	S68	6.8	10	61	7.00	21.12
S25	5	8	59	4.00	15.05	S69	10	13.2	40	1.00	25.00
S26	8	23.2	64	5.00	17.47	S70	13.2	21.25	63	8.00	22.57
S27	23.2	60.9	67	12.00	26.97	S71	22.55	32.6	70	18.00	31.38
S28	60.9	65	46	3.00	11.92	S72	32.6	35.15	64	9.00	23.85
S29	65	100	69	17.00	30.76	S73	35.15	60	71	21.00	33.05
S30	100	140.1	66	12.00	26.97	S74	10.4	30	42	1.00	22.00
S31	140.1	158	71	20.00	32.52	S75	35	40.35	56	4.00	15.05
S32	158	180	71	20.00	32.52	S76	40.35	47.7	61	6.50	20.32
S33	5	80	66	14.00	28.65	S77	47.7	51.4	50	2.00	7.52
S34	80	85	52	3.00	11.92	S78	51.4	67.1	76	22.00	33.56
S35	85	192.7	69	17.00	30.76	S79	67.1	120	66	12.00	26.97
S36	192.7	203	52	3.00	11.92	S80	72.9	80	45	1.00	22.00
S37	203	211.9	63	8.50	23.23	S81	80	97.95	66	12.00	26.97
S38	211.9	215	51	2.50	9.94	S82	97.95	300	69	16.00	30.10
S39	215	280	56	4.00	15.05	S83	3.6	30	71	20.00	32.52
S40	5	15	52	3.00	11.92	S84	4.4	6.3	50	2.00	7.52
S41	15	22.3	67	13.00	27.84	S85	6.3	60	61	7.00	21.12
S42	22.3	31.2	67	13.00	27.84	S86	6.7	24.9	68	15.00	29.40
S43	31.2	60	69	18.00	31.38	S87	76.4	90	64	14.00	28.65
S44	5	15	59	5.00	17.47						

(a) **(b)**

Fig. 3 Examples of the core boxes: (a) right abutment, and (b) left abutment.

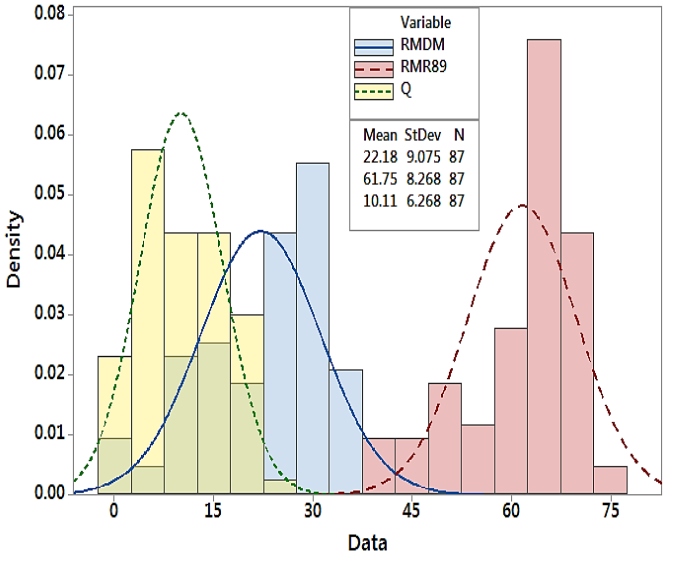

Fig. 4 Histogram of RMDM, RMR89, and Q.

in Fig. 3. The histogram of the variables shows that it is possible to perform statistical analysis and multivariate regression on the data (Fig. 4). Rock masses are categorized into three groups based on RMDM obtained from dilatometric tests, as outlined in Table 5.[65] The left abutment of the site falls into the first group with an average RMDM of 19.88 GPa. Also, the right abutment, with a mean RMDM of 20.53 GPa, is classified in the first group.**Table 5.** Rock mass classification based on RMDM.[65]

Descriptions	RMDM (GPa)	Group
No need for additional tests.	RMDM > 10	1
Needs more test assessment.	5 < RMDM < 10	2
Needs in-situ tests.	RMDM < 5	3

The dam site's rock masses, assessed through exploratory studies and RMR classification, yielded geological strength index (GSI) values of 50 ± 5, 65 ± 5, and 60 ± 5 for the Gachsaran formation, right and left abutments respectively. The mean values of the Q, RMR, and RQD are presented in Fig. 5.

3.3 Hoek-Brown and shear strength parameters

Triaxial tests were conducted under saturated conditions to estimate the shear strength parameters and obtain the necessary values for Hoek-Brown's failure criterion.[45] Lateral pressures were determined considering lithology, depth, and position, following Hoek-Brown's[45] recommendations. These failure curves for intact rock at the site were drawn based on experimental results (an example in Fig. 6). Subsequently, the fixed parameters (*i.e.*, m_i and s) for the Hoek-Brown failure criterion of the intact rock were calculated using the results of triaxial experiments (Fig. 6).

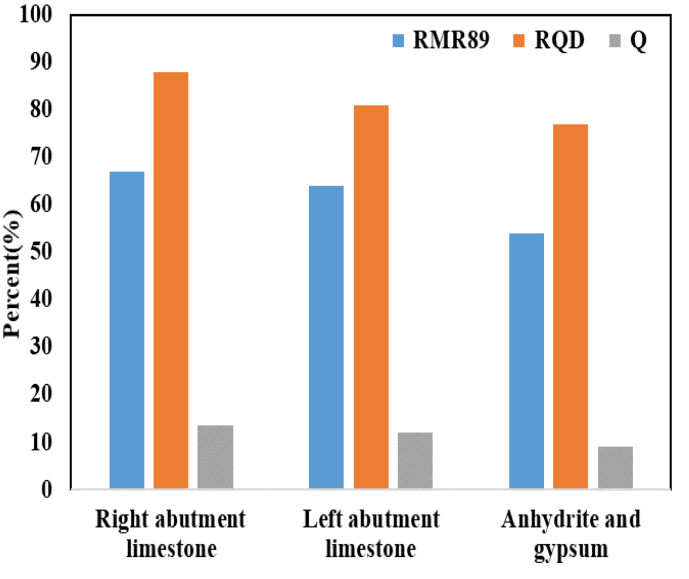

Fig. 5 Results of rock mass classifications.

In terms of shear strength parameters, Hoek-Brown[45] established failure criterion values for the site rock masses, as

Table 6. Evaluation results of previous and current relationships.

Equation (Eq.)	Results of evaluation criteria				Eq. number	References
	R^2	RMSE	VAF%	PI		
RMR89=8.7*LN(Q)+ 38.02	0.93	6.36	92.49	-4.51	(43)	Kaiser and Gale[68]
RMR89=6.64*LN(Q)+32.75	0.94	15.77	93.79	- 13.89	(44)	Hassanpour *et al.*[69]
RMR89=5.80*LN(Q)+54.41	0.94	5.86	93.58	-3.98	(45)	Wijaya *et al.*[67]
RMR89=12.33*LN(Q)+26.00	0.94	10.98	93.87	-9.10	(46)	Sadeghi *et al.*[70]
RMR89=9*LN(Q)+44.02	0.94	2.20	93.44	-0.32	(47)	Bieniawski[4]
RMR89=4.54*LN(Q)+46.34	0.94	7.73	93.95	-5.85	(48)	Sayeed and Khanna[66]
RMR89=9.57*LN(Q) + 42.20	0.95	0.36	94.95	+1.54	(49)	This study

detailed in Fig. 7. To determine internal friction angle (Φ) and cohesion (c) using the Mohr-Coulomb criterion, these parameters were calculated at various stress levels, resulting in the shear strength parameters outlined in Fig. 7.

3.4 Relationship between RMR89 and Q

After removing outlier data from 18 boreholes, Fig. 8 illustrates a robust correlation between Q and RMR89 classifications. A notable correlation, predominantly expressed through a logarithmic function, is evident. The present study results are also in harmony with the findings of earlier researchers regarding the superiority of the logarithmic relationship.[66,67] Evaluation of earlier relationships (Table 6 and Fig. 9) reveals high coefficients of determination but significant error values. Previous researchers have also stated that these errors necessitate the development of local relationships for each site.[67,68]

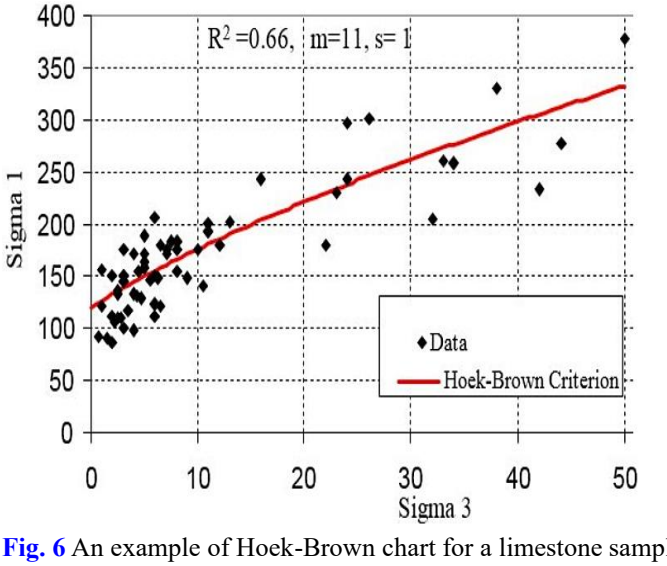

Fig. 6 An example of Hoek-Brown chart for a limestone sample.

3.5 Simple regression to estimate RMDM

The estimation of RMDM is essential for evaluating the deformation behavior and stability of rock masses in geotechnical engineering. This study provides an assessment of recent studies that have focused on various empirical methods and models for estimating the RMDM. To investigate the effect of the geomechanical parameters of the site on the RMDM, the correlation matrix (Table 7) and the two-variable regression model (Table 8) were examined separately. Results showed that it is possible to estimate the RMDM. Then, by forming linear and non-linear multivariate regression methods, the effects of parameters were studied to determine the best equation for estimating the RMDM.

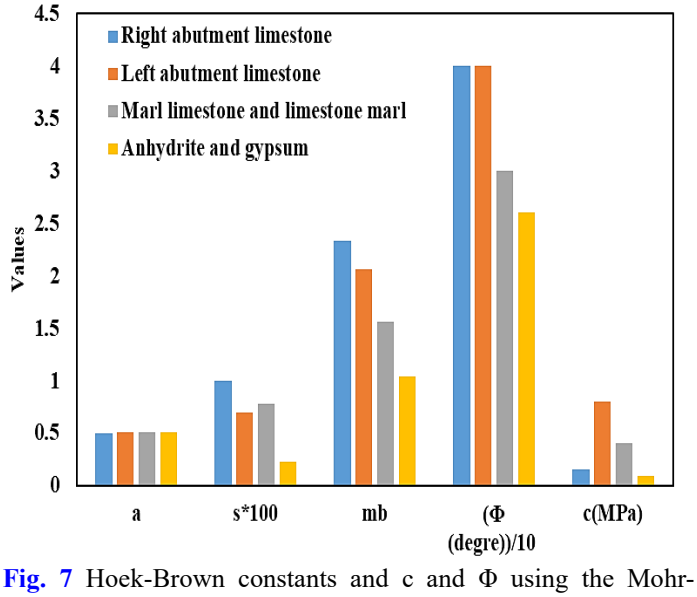

Fig. 7 Hoek-Brown constants and c and Φ using the Mohr-Coulomb criterion for the site.

To provide relations to estimate the RMDM, Minitab software was used, which, in addition to its ease of use, is one of the most powerful tools for statistical analysis of data. At the beginning of the analysis, univariate and multivariate regression modeling were used, and then the following tests were used to determine the power of the methods to process the data.

1) R-square (R^2) to analyze the dependence of the presented relationship with the tested values.

2) Durbin-Watson's (DW) test to check the non-correlation of errors
3) Checking the significance of the relationships and the non-randomness of the values of the independent parameters with the help of F and t-tests and checking these tests with the Sig statistic.
4) Checking the normality chart and the histogram of the remaining errors.

Table 7. Correlation matrix results.

	RMDM	RMR89	Q
RMDM	1		
RMR89	0.97	1	
Q	0.93	0.87	1

Table 8. Relationship between RMDM and rock mass classification systems with different functions.

RMDM versus RMR89	R^2	RMSE	Eq. No.	RMDM versus Q	R^2	RMSE	Eq. No.
$y = -0.08 x^2 + 3.12 x + 2.08$	0.97	0.10	(50)	$y = 0.00 x^2 + 0.75 x - 34.31$	0.94	0.13	(55)
$y = 1.34 x + 8.61$	0.87	0.18	(51)	$y = 1.06 x - 43.16$	0.94	0.14	(56)
$y = 5.79 e^{0.11 x}$	0.63	0.26	(52)	$y = 0.03 e^{0.11 x}$	0.61	0.19	(57)
$y = 1.91 x^{1.08}$	0.64	0.21	(53)	$y = 0.00 x^{6.18}$	0.65	0.35	(58)
$y = 10.81 \ln(x) + 0.11$	0.99	0.08	(54)	$y = 59.67 \ln(x) - 223.22$	0.94	0.11	(59)

3.6 Multivariate linear regression (MVLR) model

Based on the MVLR results, the values of the coefficient of determination and the adjusted coefficient of determination are equal to 0.96 and 0.96, respectively (Table 9). The DW statistic is equal to 1.72, which means that the errors are uncorrelated. From the value of the Sig. statistic, it can be concluded that the relationship presented is not random and is significant in this respect.

According to the analysis of variances (ANOVA) in Table 10, it can be seen that the independent parameters used in the relationship have the ability to explain and justify approximately 96% of the variance of the acceptable deformation modulus, and the rest is dependent on other parameters (of course, 96% is an acceptable value). The ANOVA and DW are used to check the applicability of the models.[64] The coefficients of the parameters are given in Table 11. Finally, the relationship presented using MVLR is in the form of Eq. (60).

$$RMDM = -28.01 + 0.7317\,RMR89 + 0.4949\,Q \quad (60)$$

The normality diagrams and error histogram are revealed in Fig. 10. This Figure displays that the error residuals are normally distributed.

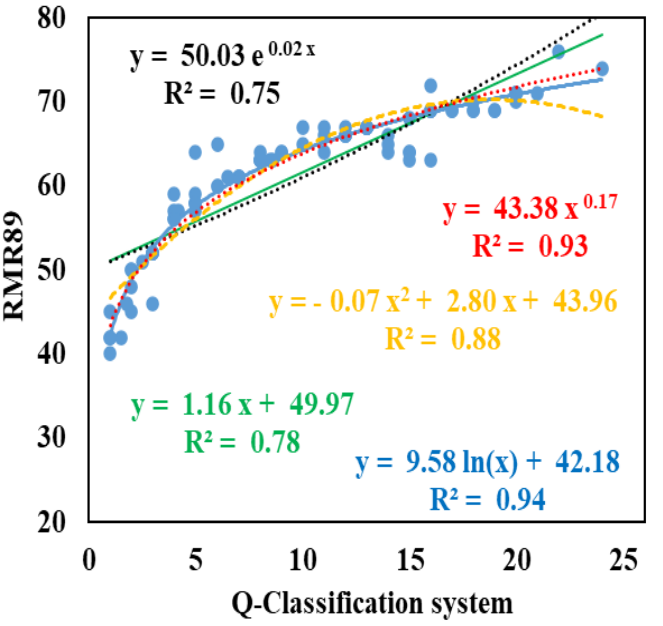

Fig. 8 Relationship between Q and RMR89.

Table 9. Evaluating criteria for the MVLR method.

S	R-sq	R-sq(adj)	RMSE	Durbin-Watson (DW) statistic
1.75	96.35%	96.26%	0.11	1.7228

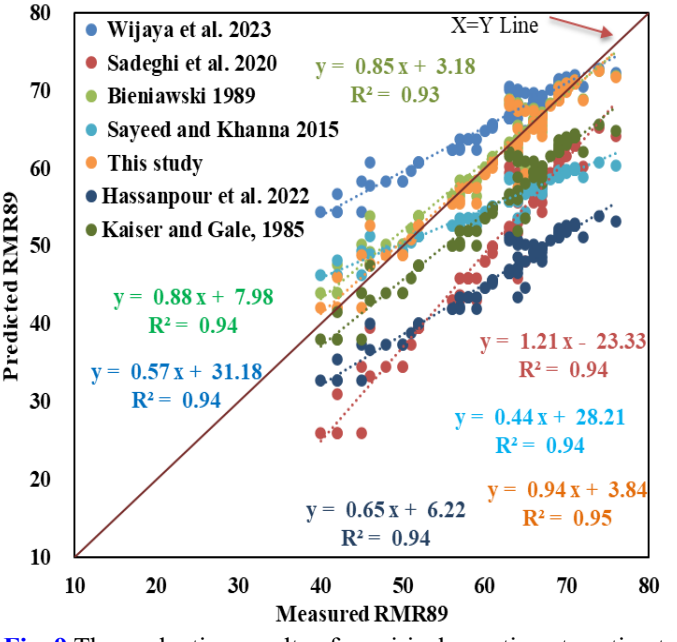

Fig. 9 The evaluation results of empirical equations to estimate RMR89.

Table 10. MVLR results of RMDM versus RMR89 and Q.

Source	DF	Seq SS	Contribution	Adj SS	Adj MS	F-Value	Sig.
Regression	2	6824.26	96.35%	6824.26	3412.13	1108.46	0.000
RMR89	1	6641.74	93.77%	693.92	693.92	225.43	0.000
Q	1	182.52	2.58%	182.52	182.52	59.29	0.000
Error	84	258.57	3.65%	258.57	3.08		
Lack-of-Fit	51	258.57	3.65%	258.57	5.07		
Pure Error	33	0.00	0.00%	0.00	0.00		
Total	86	7082.84	100.00%				

Table 11. Coefficients of the parameters.

Term	Coef	SE Coef	95% CI	T-Value	P-Value
Constant	-28.01	2.46	(-32.90, -23.11)	-11.38	0.000
RMR89	0.7317	0.0487	(0.6347, 0.8286)	15.01	0.000
Q	0.4949	0.0643	(0.3671, 0.6228)	7.70	0.000

3.7 Multivariate non-linear regression (MVNLR) model

In the investigations, it was found that the logarithmic model has a higher coefficient of determination than the linear model. Therefore, the research was conducted on non-linear models. In the combined model to form the equation according to the type of variables, an exponential function is used to model the variables. According to Table 12, the value of the coefficient of determination is equal to 0.97. In this model, the assumption of non-correlation of errors (the value of the DW statistic between 1.5 and 2.5) is established. According to Table 12 and Fig. 11, the independent parameters are effective in determining the dependent parameter. Also, according to the Sig. statistic, the presented relationship is significant, and it can be concluded that the relationship was not chosen randomly. Finally, the presented MVNLR is in the form of Eq. (61).

3.8 MLPBPANN and KNN modeling results

In this study, an MLPBPANN of the feed-forward type was employed. The input layer consisted of 2 neurons, corresponding to the independent variables utilized. The output layer was defined based on the desired outputs. The determination of the hidden layers and the number of neurons within them depended on the complexity of the problem at

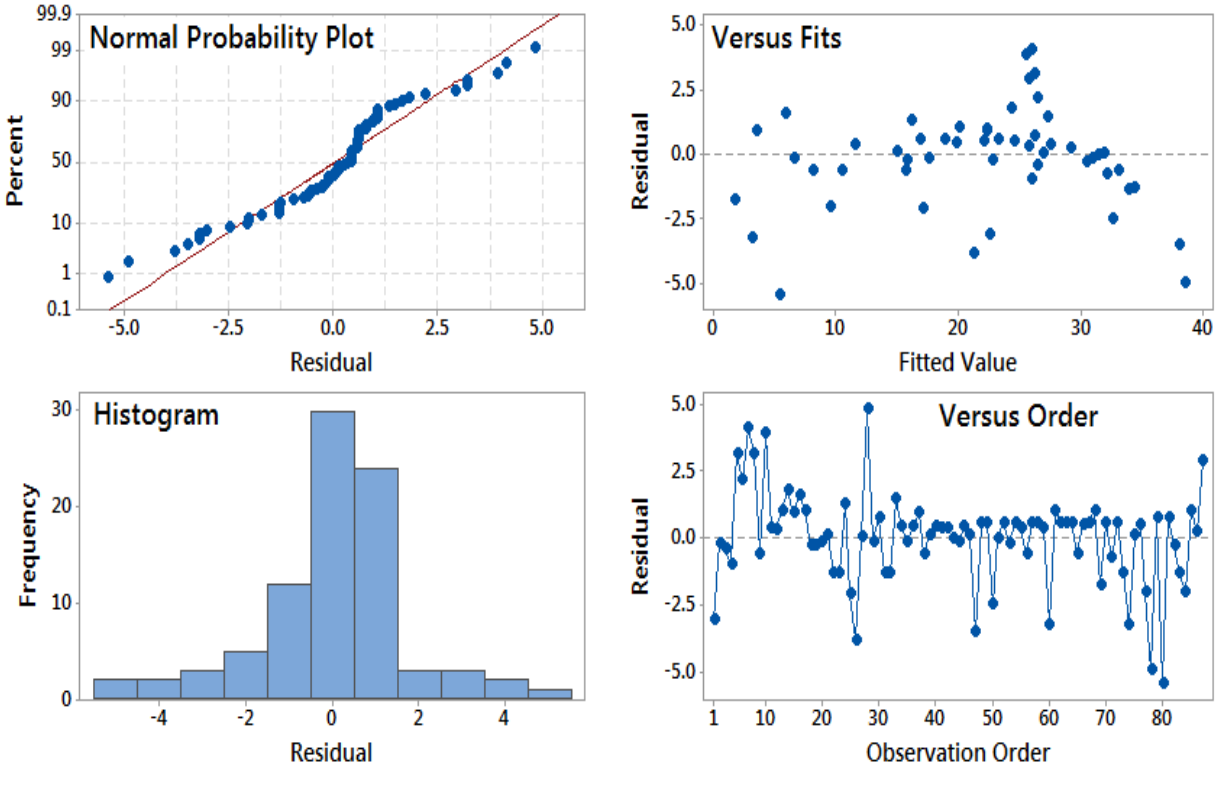

Fig. 10 Histogram of errors of residuals of the relationship provided by MVLR.

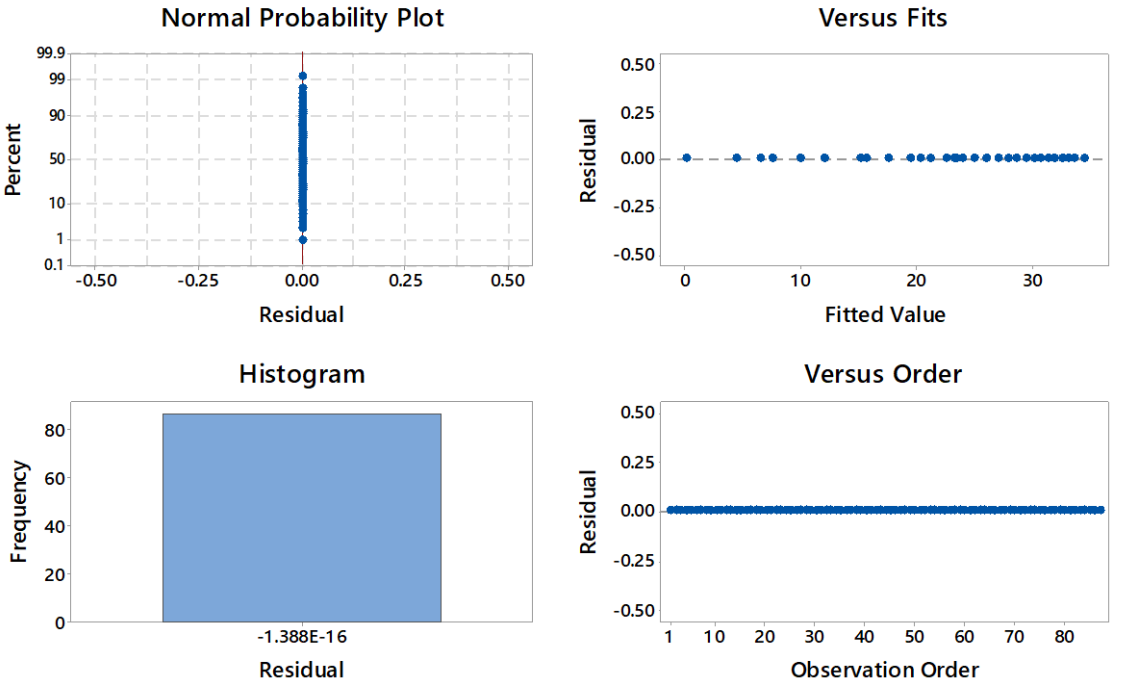

Fig. 11 Diagrams of MVNLR model residuals.

Table 12. The MVNLR results.

Equation	R^2	RMSE	DW	P-value	Max. iterations	Used algorithm	Tolerance	Eq. No.
RMDM = 3.61e14*Ln(RMR89)+ 10.86*Ln(Q)	0.97	0.11	1.8	0.00	200	Gauss-Newton	0.00001	(61)

hand.[71] Generally, a single hidden layer with a minimal number of neurons was favored. For the MLPBPANN, like other methods, the data were randomly divided into two groups: training (75% of the total data) and testing (25% of the total data). The training group was used to train the data and determine the weights, and the testing group was employed to evaluate the model.[72,73] To assess the efficiency of the training algorithms, namely LM (Levenberg-Marquardt), BR (Bayesian regularization), and SCG (scald conjugate gradient), in estimating the RMDM using MLPBPANN, various combinations and varying numbers of neurons in a single hidden layer were employed, as shown in Fig. 12. The best model is characterized using correlation coefficient and error rate.[74,75]

These choices were based on the recommendations of previous researchers. The aforementioned process was carried out for neurons 1 to 3, utilizing the equations presented earlier (Table 13). Then, based on the statistical criteria the optimal model for forecasting RMDM was identified.

In all of the training algorithms presented in Table 14, a

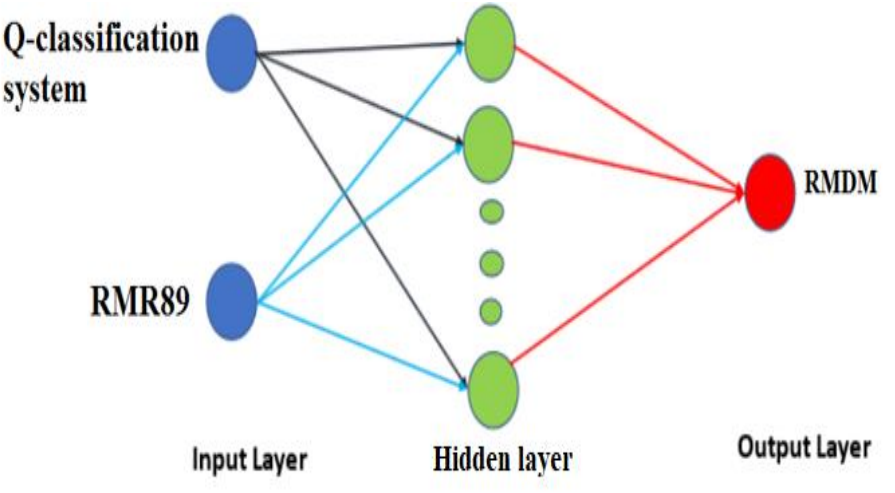

Fig. 12 The MLPBPANN structure used in this research.

Table 13. Hidden layer number estimation.

References	Equations	Neuron numbers calculated in current research	Eq. no.
Hecht-Nielsen[76]	$\leq 2 * y + 1$	≤3	(62)
Hush[77]	$3 * y$	3	(63)
Ripley[78]	$(y + x)/2$	1.5	(64)
Paola[79]	$\frac{2 + y * x + 0.5x * (x\text{^}2 + y) - 3}{(y + x)}$	2	(65)
Wang[80]	$2y/3$	0.67	(66)

x and *y* are the numbers of input and output neurons, respectively

sigmoid transfer function was applied between the input layer and the hidden layer, while a linear transfer function was utilized between the hidden layer and the output layer. In this study, the LM algorithm yielded the most accurate outcomes when estimating RMDM for the first neuron, as depicted in Figs. 13 and 14. The LM algorithm possesses the fastest convergence rate when addressing technical and engineering problems.[50,5] One advantage of this algorithm is its ability to adaptively adjust the learning rate within the network.[81,82] The results indicate that the accuracy of the test data was equal to or greater than that of the training data, suggesting the absence of overfitting in the models. Furthermore, the validation data produced results with an accuracy close to one, further confirming the absence of overfitting in the model outcomes. In this study, the results obtained from the MLPBPANN for forecasting RMDM were compared to the GPR, KNN, and RF methods.

Table 14. Results of MLPBPANN using LM, BR, and SCG training algorithms.

Optimal MLPBPANN	Activation functions	Training functions	R (for test data)	RMSE (for test data)
2*1*1	Tansig, linear	LM	0.97	0.03
2*2*1	Tansig, linear	SCG	0.95	0.05
2*1*1	Tansig,linear	BR	0.96	0.05

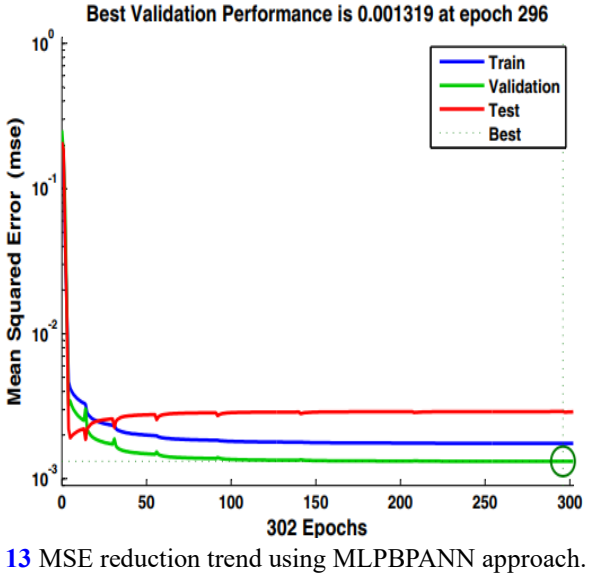

Fig. 13 MSE reduction trend using MLPBPANN approach.

In the KNN approach, optimal neighbors are selected using distance metrics.[47] In the current study, we chose the Euclidean distance metric. Fig. 15 shows the training error curve for different K values when estimating RMDM. As can be seen, the optimum K value for estimating RMDM equals 3. Importantly, the KNN model outperformed multivariate methods in forecasting RMDM.

3.9 Results of GPR and RF methods

The GPR model confirmed acceptable performance by precisely forecasting the majority of RMDM values, with the predicted values closely aligned with the actual values (Fig. 16). MLPBPANN follows the empirical risk minimization (ERM) principle. The ERM principle seeks to minimize the incorrect classification error or deviation from the correct solution of training data.[47] The RF modeling process was executed utilizing R software (R.4.2.1). Like other ML methods used in this research, in the RF method, 25% of the total samples were used for model training, and 75% of the total samples were also used for model evaluation. This learning method, which is based on a group of decision trees using bootstrap samples and subsets of random features, shows high flexibility against overfitting.[47] In the current study, to determine the optimal number of parameters and nodes in each tree, a 10-fold cross-validation approach was implemented. Consequently, the RF method produced optimal outcomes with 520 trees and two variables in each node. In summary, when evaluating the precision of RF, GPR, and MLPBPANN, it's important to consider factors such as dataset characteristics, training algorithms, learning rate, and the specific problem at hand.

3.10 Evaluation of used models and previous relationships

Many relationships have been proposed by previous researchers to estimate RMDM (Table 1). RMDM values were estimated based on previous and current relationships and models, and their correlation with the measured RMDM values at the Khersan dam site was checked. The evaluating results of previous equations and developed models in the current research are presented in Fig. 17. In this figure, parts a, b, and c show the correlation between measured RMDM and predicted RMDM based on previous relationships and developed models in the current study. The RMSE and R-squared are commonly used to assess the predictive

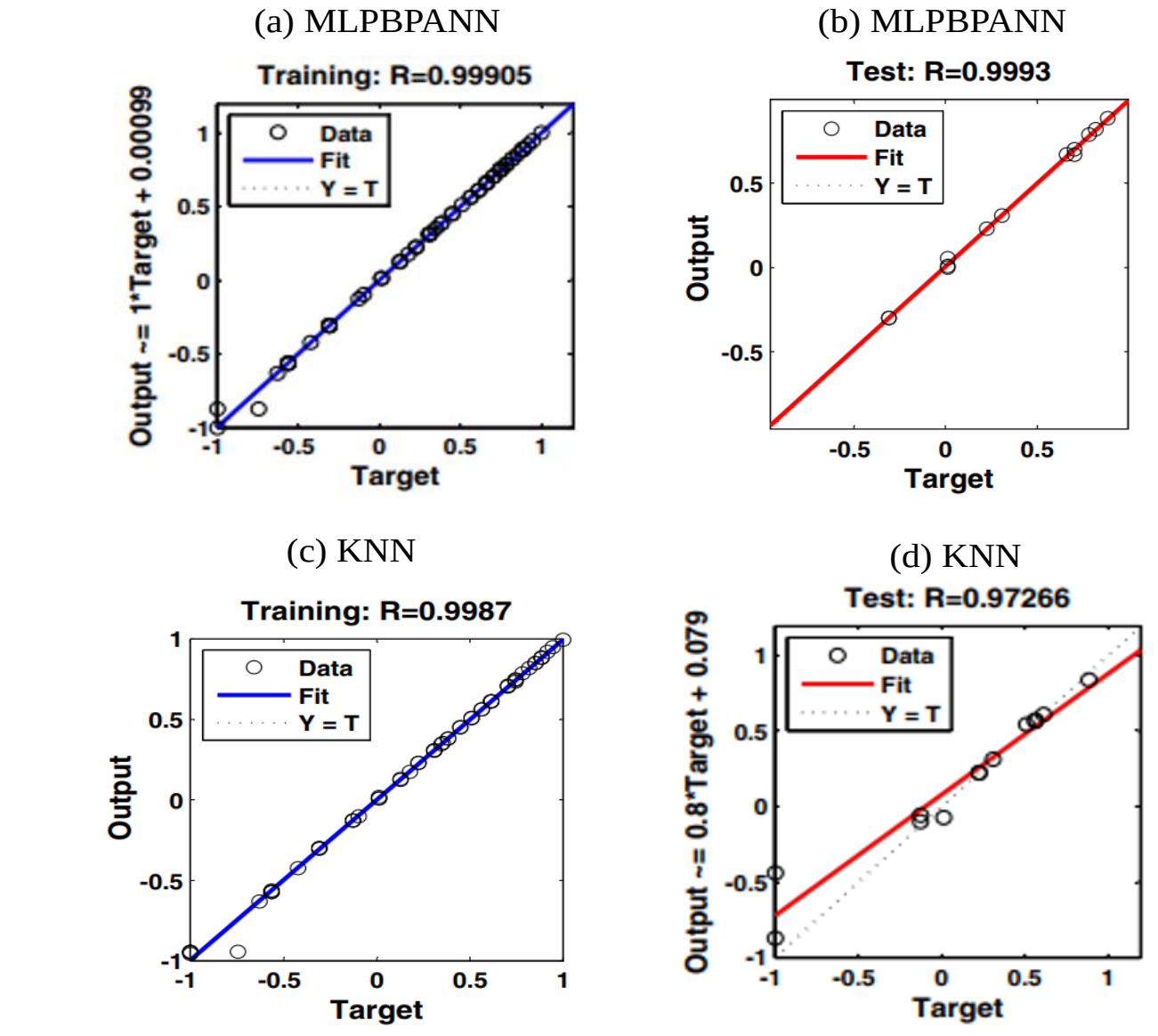

Fig. 14 The MLPBPANN and KNN results in RMDM estimation.

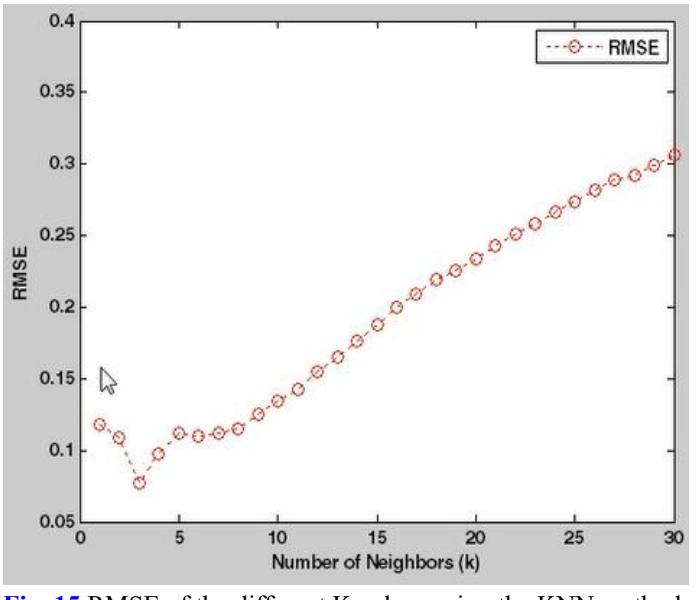

Fig. 15 RMSE of the different K values using the KNN method.

performance of models in prediction tasks.[83,84] Fig. 17d depicts the MAPE and PI, which are used to assess the efficiency of the achieved models in the current research.

Based on the correlation coefficient, it can be seen that some of the relationships are accurate enough to estimate RMDM. The findings presented in Fig. 17 reveal that the equation presented by Palmström and Singh[36] has a higher accuracy in predicting the deformation modulus compared to other equations from the research background. Meanwhile, machine learning (ML) methods are the most accurate.

The mean estimated RMDM value obtained using the GPR was found to be lower than the corresponding real values (Fig. 18). This indicates that the GPR tends to be conservative in RMDM estimation. In contrast, the RF, KNN, MVLR, MVNLR, and MLPBPANN approaches do not exhibit conservative behavior when estimating RMDM. Fig. 18b shows the relationship between the error level and the accumulated frequency. As can be seen, the newly developed

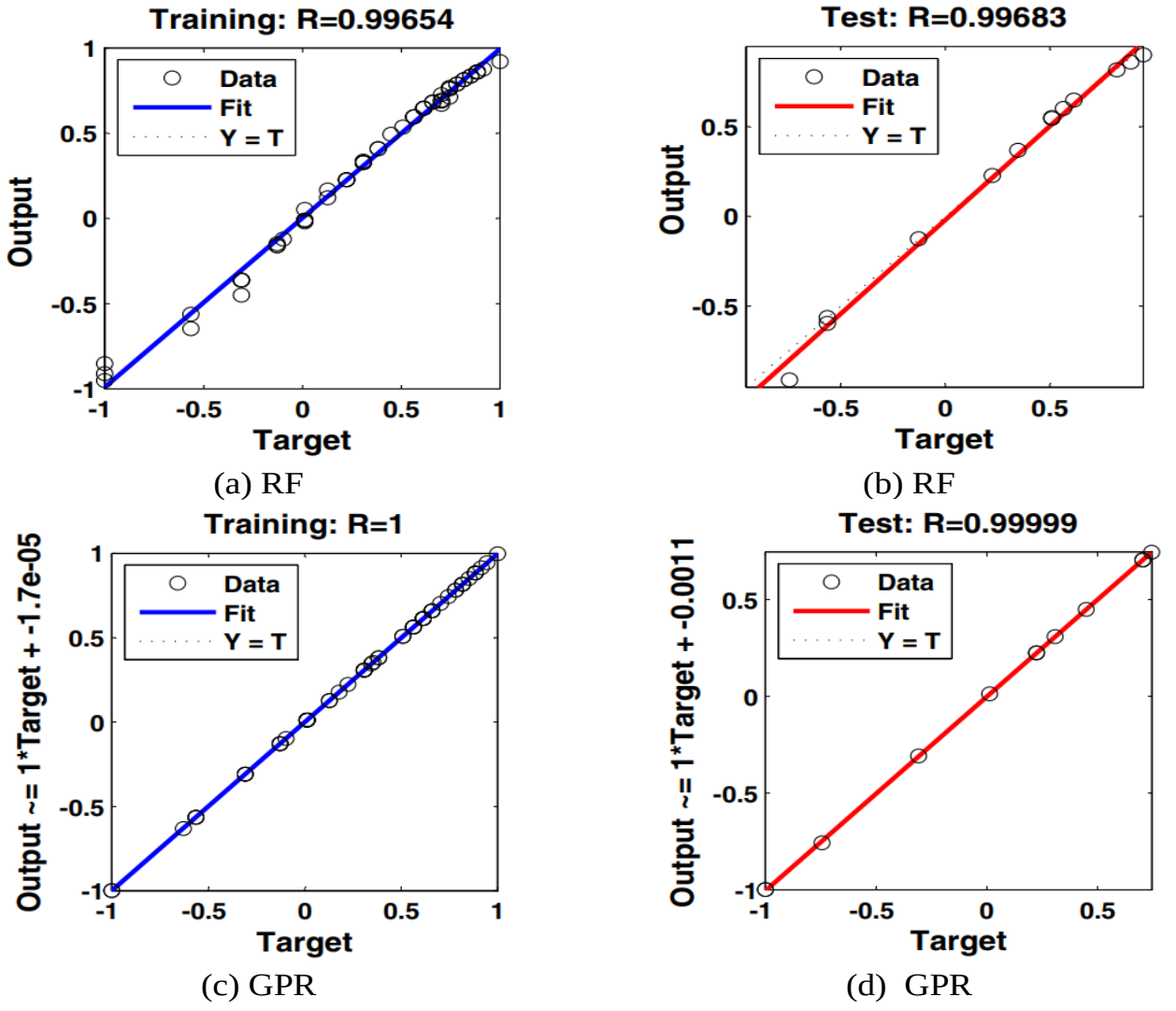

Fig. 16 RMDM modeling results using GPR and RF methods.

models in the current study show lower error levels with a higher cumulative frequency as compared with previous empirical equations. Previous researchers have used this method to evaluate empirical relationships.[85]

3.11 Research limitations

There are some limitations that need to be resolved as much as possible in future research. This study used the Q and RMR89 classification systems to estimate RMDM. Although these classification systems include the major characteristics of the rock mass, including the characteristics of the joints, some characteristics, such as the elastic modulus of the intact rock and the joint apertures, were not included. Therefore, it is better to include other factors affecting RMDM. In this study, 87 data points from 19 exploratory boreholes were used. It is necessary to use more data in future research to increase the accuracy and reliability of the models. In addition, the performance of intelligent methods can be improved by using optimization techniques such as genetic algorithms, etc. Finally, the performance of other models such as support vector machine, ANFIS (adaptive neuro-fuzzy inference system), decision trees, genetic algorithm, etc. should also be investigated and compared using various statistical criteria.

4.Conclusions

Estimating the deformation modulus of rock masses is a challenging task due to the complex nature of rock mass behavior. The reviewed studies have contributed to the understanding and estimation of RMDM through various empirical methods. These approaches consider factors such as intact rock properties, discontinuity characteristics, rock mass classifications, and site-specific conditions. Further research in this field is necessary to enhance the accuracy and reliability of estimation methods and to address the diverse range of rock mass conditions encountered in geotechnical projects. In this research, the RMDM of the Khersan-2 dam site was estimated based on 88 data points from the dilatometry test results and the geo-mechanical properties of the rock mass. According to the Q and RMR classification systems, the site was generally placed in the good category. Hoek-Brown constants, cohesion, and friction angle achieved from the Mohr-Coulomb criterion were determined for the site. A new relationship with high

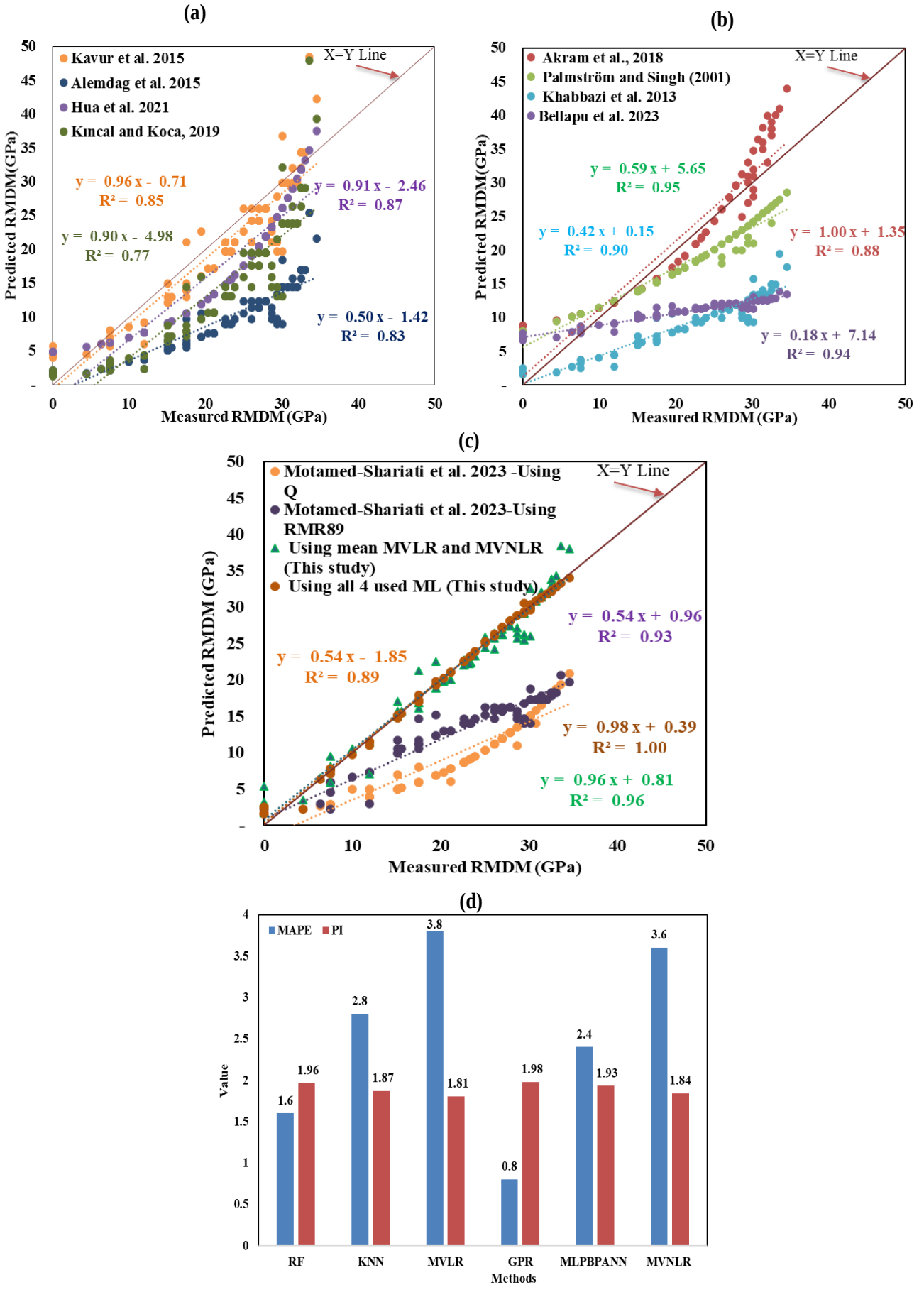

Fig. 17 Accuracy and dispersion of measured and estimated RMDM values.

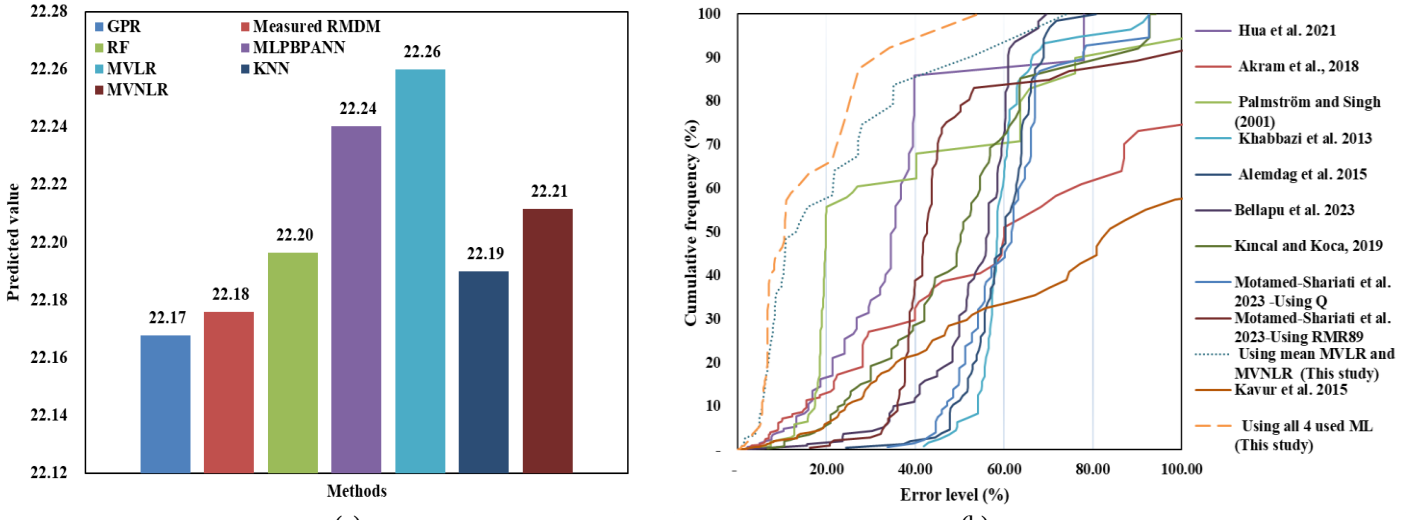

Fig. 18 Mean of estimated RMDM using statistical and machine learning methods versus measured values (a), and error level versus cumulative frequency (b).

precision (R^2 = 0.95, RMSE = 0.36, VAF% = 94.95, and PI =+1.54) was established between Q and RMR89. To find the relationships that have the best ability to calculate the modulus of deformation, simple and multiple regression modeling were done in linear and non-linear forms. From the statistical results, it was found that regression models with high accuracy are effective for estimating RMDM. Among the models, the power and logarithmic models have the highest values of the coefficient of determination to estimate the RMDM. In multivariable models, the non-linear model with a coefficient of determination of 0.97 has the most accuracy and is significant in terms of all the statistical tests performed. Artificial intelligence models were able to estimate RMDM with higher accuracy than statistical methods. The GPR method, having the highest accuracy (R^2=0.99, RMSE=0.01, and PI=+1.98) compared to other methods, acted conservatively in estimating RMDM. Also, among the training algorithms of the MLPBPANN, the Levenberg-Marquardt algorithm showed the highest accuracy. The presented models for predicting RMDM are suitable for other areas when the values of the predictive indicators are in the same range as this study. It is recommended that future research be conducted using a larger dataset in order to enhance the accuracy of predictions.

Acknowledgement

This study was supported by Thammasat Postdoctoral Fellowship. This research budget was allocated by National Science, Research and Innovation Fund (NSRF) and King Mongkut's University of Technology North Bangkok (Project no. KMUTNB-FF-67-A-05).

Conflict of Interest

There is no conflict of interest.

Supporting Information

Not applicable.

References

[1] A. Rastegarnia, G. R. Lashkaripour, M. Ghafoori, S. S. Farrokhad, Assessment of the engineering geological characteristics of the Bazoft Dam site, SW Iran, *Quarterly Journal of Engineering Geology and Hydrogeology*, 2019, **52**, 360-374, doi: 10.1144/qjegh2017-042.

[2] E. Sharifi Teshnizi, M. Golian, S. Sadeghi, A. Rastegarnia, Application of analytical hierarchy process (AHP) in landslide susceptibility mapping for Qazvin Province, N Iran. *Computers in Earth and Environmental Sciences*, 2022, 55-95, doi: 10.1016/b978-0-323-89861-4.00041-5.

[3] F.-Y. Jiao, H.-D. Wang, T. Li, Y. Chen, G.-W. Ma, Multi-domain equivalent method for prediction of elastic modulus of complex fractured rock mass, *Journal of Mountain Science*, 2023, **20**, 859-872, doi: 10.1007/s11629-022-7387-5.

[4] Z. Bieniawski, Engineering rock mass classifications: a complete manual for engineers and geologists in mining, civil, and petroleum engineering, John Wiley & Sons, 1989.

[5] B. Ghoreishi, M. K. Esfahani, N. A. Lushabi, O. Amini, I. Aghamolaie, N. A. A. N. Hashim, S. M. S. Alizadeh, Correction to: assessment of geotechnical properties and determination of shear strength parameters, *Geotechnical and Geological Engineering*, 2021, **39**, 479, doi: 10.1007/s10706-020-01528-7.

[6] A. Rastegarnia, A. Sohrabibidar, V. Bagheri, M. Razifard, and A. Zolfaghari Assessment of relationship between grouted values and calculated values in the Bazoft Dam Site, *Geotechnical and Geological Engineering*, 2017, **35**, 1299-310, doi: 10.1007/s10706-017-0176-1.

[7] H. V. S. Bellapu, R. K. Sinha, S. R. Naik, Estimation of modulus of deformation using rock mass rating—a review and validation using 3D numerical modelling, *Sustainability*, 2023, **15**, 5721, doi: 10.3390/su15075721.

[8] M. Hasanipanah, M. Jamei, A. S. Mohammed, M. N. Amar, O. Hocine, K. M. Khedher, Intelligent prediction of rock mass deformation modulus through three optimized cascaded forward neural network models, *Earth Science Informatics*, 2022, **15**, 1659-1669, doi: 10.1007/s12145-022-00823-6.

[9] E. Emami Meybodi, A. DastBaravarde, S. K. Hussain, S. Karimdost, Machine-learning method applied to provide the best predictive model for rock mass deformability modulus (Em), *Environmental Earth Sciences*, 2023, **82**, 149, doi: 10.1007/s12665-023-10815-4.

[10] E. Motamed-Shariati, M. Motevalizadeh, E. S. Teshnizi, Estimation of rock mass deformability based on empirical relations for Ghezel Ozan Dam site in the north of Iran, *Quarterly Journal of Engineering Geology and Hydrogeology*, 2023, **56**, 138, doi: 10.1144/qjegh2021-138.

[11] A. E. Aladejare, T. Malachi Ozoji, M. Adebayo Idris, A. I. Lawal, M. Onifade, Empirical estimation of rock mass deformation modulus of rocks: comparison of intact rock properties and rock mass classifications as inputs, *Arabian Journal of Geosciences*, 2022, **15**, 1033, doi: 10.1007/s12517-022-10190-7.

[12] D. Chen, H. Chen, W. Zhang, J. Lou, B. Shan, An analytical solution of equivalent elastic modulus considering confining stress and its variables sensitivity analysis for fractured rock masses, *Journal of Rock Mechanics and Geotechnical Engineering*, 2022, **14**, 825-836, doi: 10.1016/j.jrmge.2021.08.007.

[13] B. Zhang, J. Mu, J. Zheng, Q. Lv, J. Deng, A new estimation method and an anisotropy index for the deformation modulus of jointed rock masses, *Journal of Rock Mechanics and Geotechnical Engineering*, 2022, **14**, 153-168, doi: 10.1016/j.jrmge.2021.06.005.

[14] K. Polemis Jr, F. C. da Silva Filho, F. P. Lima-Filho, Estimating the rock mass deformation modulus: a comparative study of empirical methods based on 48 rock mass scenarios, *REM - International Engineering Journal*, 2021, **74**, 39-49, doi: 10.1590/0370-44672019740150.

[15] D. Hua, Q. Jiang, R. Liu, Y. Gao, M. Yu, Rock mass deformation modulus estimation models based on *in situ* tests, *Rock Mechanics and Rock Engineering*, 2021, **54**, 5683-5702, doi: 10.1007/s00603-021-02578-w.

[16] X. Que, Z. Zhu, Z. Niu, W. Lu, Estimating the strength and deformation of columnar jointed rock mass based on physical model test, *Bulletin of Engineering Geology and the Environment*, 2021, **80**, 1557-1570, doi: 10.1007/s10064-020-01974-w.

[17] M. Koopialipoor, P. G. Asteris, A. Salih Mohammed, D. E. Alexakis, A. Mamou, D. J. Armaghani, Introducing stacking machine learning approaches for the prediction of rock deformation, *Transportation Geotechnics*, 2022, **34**, 100756, doi: 10.1016/j.trgeo.2022.100756.

[18] S. Alemdag, Z. Gurocak, C. Gokceoglu, A simple regression based approach to estimate deformation modulus of rock masses, *Journal of African Earth Sciences*, 2015, **110**, 75-80, doi: 10.1016/j.jafrearsci.2015.06.011.

[19] J. Gholamnejad, H. Bahaaddini, M. Rastegar Prediction of the deformation modulus of rock masses using Artificial Neural Networks and Regression methods, *Journal of Mining and Environment*, 2013, **4**, 35-43, doi: 10.22044/jme.2013.144.

[20] K. Tokgozoglu, C. H. Aladag, C. Gokceoglu, Artificial neural networks to predict deformation modulus of rock masses considering overburden stress, *Geomechanics and Geoengineering*, 2023, **18**, 48-64, doi: 10.1080/17486025.2021.2008518.

[21] H. R. Nejati, A. Ghazvinian, S. A. Moosavi, V. Sarfarazi, On the use of the RMR system for estimation of rock mass deformation modulus, *Bulletin of Engineering Geology and the Environment*, 2014, **73**, 531-540, doi: 10.1007/s10064-013-0522-3.

[22] B.-S. Chun, W. R. Ryu, M. Sagong, J.-N. Do, Indirect estimation of the rock deformation modulus based on polynomial and multiple regression analyses of the RMR system, *International Journal of Rock Mechanics and Mining Sciences*, 2009, **46**, 649-658, doi: 10.1016/j.ijrmms.2008.10.001.

[23] S. Barami, M. Behnia, Experimental and numerical investigations on the effect of *in situ* stress and discontinuities orientation on the deformation modulus of rock masses, *International Journal of Geomechanics*, 2024, **24**, 04023287, doi: 10.1061/ijgnai.gmeng-9178.

[24] K. Karaman, F. Cihangir, A. Kesimal, A comparative assessment of rock mass deformation modulus, *International Journal of Mining Science and Technology*, 2015, **25**, 735-740, doi: 10.1016/j.ijmst.2015.07.006.

[25] E. J. Lindenbach, S. C. Dalton, R. G. Bearce, G. D. Arany, A Comparison Between Field-Measured and Empirically Estimated Rock Mass Modulus Values All Days. June 26-29, 2022. Santa Fe, New Mexico, USA. ARMA, 2022.

[26] S. Panthee, P. Singh, A. Kainthola, R. Das, T. Singh, Comparative study of the deformation modulus of rock masses—a reply to the comments received from Gokceoglu, *Bulletin of Engineering Geology and the Environment*, 2018, **77**, 763-766, doi: 10.1007/s10064-018-1272-z.

[27] S. Radovanović, V. Ranković, V. Anđelković, D. Divac, N. Milivojević, Development of new models for the estimation of deformation moduli in rock masses based on *in situ* measurements, *Bulletin of Engineering Geology and the Environment*, 2018, **77**, 1191-1202, doi: 10.1007/s10064-017-1027-2.

[28] M. Noorian-Bidgoli, Strength and deformability of fractured rocks, 2014.

[29] M. Sari, The stochastic assessment of strength and deformability characteristics for a pyroclastic rock mass, *International Journal of Rock Mechanics and Mining Sciences*, 2009, **46**, 613-626, doi: 10.1016/j.ijrmms.2008.07.007.

[30] J. Ching, K.-K. Phoon, Y.-H. Ho, M.-C. Weng, Quasi-site-specific prediction for deformation modulus of rock mass, *Canadian Geotechnical Journal*, 2020, **58**, 1-16, doi: 10.1139/cgj-2020-0168.

[31] H. Fattahi, A. Moradi, A new approach for estimation of the rock mass deformation modulus: a rock engineering systems-based model, *Bulletin of Engineering Geology and the*

Environment, 2018, **77**, 363-374, doi: 10.1007/s10064-016-1000-5.
[32] A. Khabbazi, M. Ghafoori, G. R. Lashkaripour, A. Cheshomi, Estimation of the rock mass deformation modulus using a rock classification system, *Geomechanics and Geoengineering*, 2013, **8**, 46-52, doi: 10.1080/17486025.2012.695089.
[33] B. Kavur, N. Štambuk Cvitanović, P. Hrženjak, Comparison between plate jacking and large flat jack test results of rock mass deformation modulus, *International Journal of Rock Mechanics and Mining Sciences*, 2015, **73**, 102-114, doi: 10.1016/j.ijrmms.2014.09.022.
[34] C. Kıncal, M. Y. Koca, Correlations of *in situ* modulus of deformation with elastic modulus of intact core specimens and RMR values of andesitic rocks: a case study of the İzmir subway line, *Bulletin of Engineering Geology and the Environment*, 2019, **78**, 5281-5299, doi: 10.1007/s10064-018-01443-5.
[35] M. S. Akram, K. Mirza, M. Zeeshan, M. A. Jabbar, Assessment of rock mass quality and deformation modulus by empirical methods along kandiah river, KPK, Pakistan, *Open Journal of Geology*, 2018, **8**, 947-964, doi: 10.4236/ojg.2018.810057.
[36] A. Palmström, and R. Singh. The deformation modulus of rock masses—comparisons between in situ tests and indirect estimates, *Tunnelling and Underground Space Technology*, 2001, **16**, 115-31, doi: 10.1016/S0886-7798(01)00038-4.
[37] J. Shen, M. Karakus, C. Xu, A comparative study for empirical equations in estimating deformation modulus of rock masses, *Tunnelling and Underground Space Technology*, 2012, **32**, 245-250, doi: 10.1016/j.tust.2012.07.004.
[38] S. Hussain, N. Muhammad Khan, M. Z. Emad, A. M. Naji, K. Cao, Q. Gao, Z. Ur Rehman, S. Raza, R. Cui, M. Salman, S. S. Alarifi, An appropriate model for the prediction of rock mass deformation modulus among various artificial intelligence models, *Sustainability*, 2022, **14**, 15225, doi: 10.3390/su142215225.
[39] S.-S. Kang, H.-Y. Kim, B.-A. Jang, Correlation of *in situ* modulus of deformation with degree of weathering, RMR and Q-system, *Environmental Earth Sciences*, 2013, **69**, 2671-2678, doi: 10.1007/s12665-012-2088-y.
[40] S. Read, N. Perrin, and L. Richards, Applicability of the Hoek-Brown failure criterion to New Zealand greywacke rocks, 1999.
[41] Z. T. Bieniawski, Determining rock mass deformability: experience from case histories, *International Journal of Rock Mechanics and Mining Sciences & Geomechanics Abstracts*, 1978, **15**, 237-247, doi: 10.1016/0148-9062(78)90956-7.
[42] J. Serafim, J. Pereira, Considerations on the geomechanical classification of Beniawski: experience from case histories. Proceedings of symposium on engineering geology and underground openings, Lisbon, 1983.
[43] M. Quds-Niroo, Geological report of engineering and rock mechanics of Khorsan 2 dam and power plant design geological report of the dam, 2010.
[44] N. Barton, R. Lien, J. Lunde, Engineering classification of rock masses for the design of tunnel support, *Rock Mechanics*, 1974, **6**, 189-236, doi: 10.1007/BF01239496.
[45] E. Hoek, E. T. Brown, Empirical strength criterion for rock masses, *Journal of the Geotechnical Engineering Division*, 1980, **106**, 1013-1035, doi: 10.1061/ajgeb6.0001029.
[46] S. S. Zulcharnaevna, K. Khansulu, S. Tolganai, S. Rita, B. Nazym, K. Gulzhanat, Y. Bolat, Z. Adamzhanova, Integrating machine learning and data analysis for predictive microbial community profiling, *Caspian Journal of Environmental Sciences*, 2023, **21**, 1209-1227, doi: 10.22124/cjes.2023.7413.
[47] Z. Fang, J. Cheng, C. Xu, X. Xu, J. Qajar, A. Rastegarnia, Comparison of machine learning and statistical approaches to estimate rock tensile strength, *Case Studies in Construction Materials*, 2024, **20**, e02890, doi: 10.1016/j.cscm.2024.e02890.
[48] M. R. Motahari, O. Amini, A. Khoshghalb, M. Etemadifar, N. Alali, Investigation of the geotechnical properties and estimation of the relative density from the standard penetration test in sandy soils (case study: north east of Iran), *Geotechnical and Geological Engineering*, 2022, **40**, 2425-2442, doi: 10.1007/s10706-021-02036-y.
[49] M. R. Motahari, O. Amini, A. Iraji, O. Mahdizadeh Gohari, M. Saffarian, Comparison of dynamic and static properties of sandstone and estimation of shear wave velocity and Poisson's ratio, *Bulletin of Engineering Geology and the Environment*, 2022, **81**, 384, doi: 10.1007/s10064-022-02867-w.
[50] A. Rastegarnia, G. R. Lashkaripour, E. Sharifi Teshnizi, M. Ghafoori, Evaluation of engineering characteristics and estimation of static properties of clay-bearing rocks, *Environmental Earth Sciences*, 2021, **80**, 621, doi: 10.1007/s12665-021-09914-x.
[51] M. Nemati, M. Tofighkhah, F. Absari, Examining the four parameters of genetic algorithm in order to obtain the best solution for transportation network design problems, *Journal of Civil Engineering and Materials Application*, 2023, **7**, 191-203, doi: 10.22034/JCEMA.2023.187703.
[52] R. Arjmandzadeh, E. S. Teshnizi, A. Rastegarnia, M. Golian, P. Jabbari, H. Shamsi, S. Tavasoli, GIS-based landslide susceptibility mapping in qazvin province of Iran, *Iranian Journal of Science and Technology, Transactions of Civil Engineering*, 2019, **44**, 619 - 647, doi: 10.1007/s40996-019-00326-3.
[53] O. Anon, Classification of rocks and soils for engineering geological mapping. Part 1: rock and soil materials, *Bulletin of Engineering Geology and the Environment*, 1979, **19**, 364-437. doi: 10.1007/BF02600503.
[54] A. Rastegarnia, M. Ghafoori, N. H. Moghaddas, G. R. Lashkaripour, H. Shojaei, Application of cuttings to estimate the static characteristics of the dolomudstone rocks, *Geomechanics and Engineering*, 2022, **29**, 65-77, doi; 10.12989/gae.2022.29.1.065.
[55] N. Lerman, L. Aronofsky, B. Aghili. Investigating the microstructure and mechanical properties of metakaolin-based polypropylene fiber-reinforced geopolymer concrete using different monomer ratios, *Journal of Civil Engineering and Materials Application*, 2021, **5**, 115-123, doi: 10.22034.2021.302140.1062.

[56] F. Bouchaala, M. Y. Ali, J. Matsushima, Estimation of seismic attenuation in carbonate rocks using three different methods: application on VSP data from Abu Dhabi oilfield, *Journal of Applied Geophysics*, 2016, **129**, 79-91, doi: 10.1016/j.jappgeo.2016.03.014.
[57] S. Ghavami, M. Rajabi, Investigating the influence of the combination of cement kiln dust and fly ash on compaction and strength characteristics of high-plasticity clays, *Journal of Civil Engineering and Materials Application*, 2021, **5**, 9-16, doi:10.22034/JCEMA.2020.250727.1040.
[58] S. Alzabeebee, Y. M. Alshkane, D. A. Mohammed, S. Keawsawasvong, Comparing 1D regression and evolutionary polynomial analyses for predicting Brazilian tensile strength of limestone in dry and saturated conditions, *Geotechnical and Geological Engineering*, 2024, **42**, 2495-2515, doi: 10.1007/s10706-023-02687-z.
[59] S. Alzabeebee, D. A. Mohammed, Y. M. Alshkane, Experimental study and soft computing modeling of the unconfined compressive strength of limestone rocks considering dry and saturation conditions, *Rock Mechanics and Rock Engineering*, 2022, **55**, 5535-5554, doi: 10.1007/s00603-022-02948-y.
[60] B. Vasarhelyi, Some observations regarding the strength and deformability of sandstones in dry and saturated conditions, *Bulletin of Engineering Geology and the Environment*, 2003, **62**, 245-249, doi: 10.1007/s10064-002-0186-x.
[61] A. Rastegarnia, S. M. S. Alizadeh, M. K. Esfahani, O. Amini, A. S. Utyuzh, The effect of hydrated lime on the petrography and strength characteristics of Illite clay, *Geomechanics and Engineering*, 2020, **22**, 143, doi: 10.12989/gae.2020.22.2.143.
[62] J. Sobhani, F. Jafarpour, F. Firozya, A. R. Pourkhorshidi, Simulated C3A effects on the chloride binding in Portland cement with NaCl and $CaCl_2$ cations, *Journal of Civil Engineering and Materials Application*, 2022, **6**, 41–54, doi: 10.22034/jcema.2022.328603.1080.
[63] A. Bagherzadeh Khalkhali, I. Safarzadeh, H. Rahimi Manbar, Investigating the effect of nanoclay additives on the geotechnical properties of clay and silt soil, *Journal of Civil Engineering and Materials Application*, 2019, **3**, 63-74, doi, 10.22034/JCEMA.2019.92088.
[64] Z. Shirnezhad, A. Azma, L. K. Foong, A. Jahangir, A. Rastegarnia, Assessment of water resources quality of a karstic aquifer in the Southwest of Iran, *Bulletin of Engineering Geology and the Environment*, 2021, **80**, 71-92, doi: 10.1007/s10064-020-01871-2.
[65] J. Charrua-Graca, Dilatometer tests in the study of the deform ability of rock masses, 1979.
[66] I. Sayeed, and R. Khanna. Empirical correlation between RMR and Q systems of rock mass classification derived from Lesser Himalayan and Central crystalline rocks. International Conference on Engineering Geology in New Millennium, 2015.
[67] B. J. Wijaya, I. W. Warmada, I. G. B. Indrawan, Correlation between GSI, RMR, and Q systems of rock masses at the construction site of spillway tunnel at Meninting Dam, Construction: The Formation of Living Environment: FORM-2022, AIP Conference Proceedings. Moscow, Russian Federation. AIP Publishing, 2023.
[68] T. Kaiser, and A. Gale, Evaluation of cost and emprical support design at BC Rail Tumbler Ridge tunnels, Canadian Tunnelling, Tunnelling Association of Canada, Wiley, New York, 1985.
[69] J. Hassanpour, A. S. Khoshkar, M. G. Farasani, A. Hashemnejad, Investigating the relationships between rock mass classification systems based on data from mechanized tunneling projects in Iran, *Bulletin of Engineering Geology and the Environment*, 2022, **81**, 147, doi: 10.1007/s10064-022-02641-y.
[70] S. Sadeghi, E. Sharifi Teshnizi, B. Ghoreishi, Correlations between various rock mass classification/characterization systems for the Zagros tunnel-W Iran, *Journal of Mountain Science*, 2020, **17**, 1790-806, doi: 10.1007/s11629-019-5665-7.
[71] S. Aboutaleb, M. Behnia, R. Bagherpour, B. Bluekian. Using non-destructive tests for estimating uniaxial compressive strength and static Young's modulus of carbonate rocks via some modeling techniques, *Bulletin of Engineering Geology and the Environment*, 2018, **77**, 1717-1728, doi: 10.1007/s10064-017-1043-2.
[72] R. Shamsashtiany, M. Ameri, Road Accidents Prediction with Multilayer Perceptron MLP modelling Case Study: Roads of Qazvin, Zanjan and Hamadan, *Journal of Civil Engineering and Materials Application*, 2018, **2**, 181-192, doi: 10.22034/JCEMA.2018.91998.
[73] A. Sisodia, A. K. Yadav, Performance analysis of IoT networks in terrestrial environment utilizing LZW data compression technique, *Review of Computer Engineering Research*, 2023, **10**, 165–181, doi: 10.18488/76.v10i4.3550.
[74] M.A. Maleki, M. Emami, Application of SVM for investigation of factors affecting compressive strength and consistency of geopolymer concretes, *Journal of Civil Engineering and Materials Application*, 2019, **3**, 101-107, doi:10.1016/j. nrjag.2014.05.001.
[75] H. G. Maabreh, K. Waheeb, A. Ryadh, S. B. Abdulghani, Z. J. Hamoodah, N. Y. Jasim, F. Alajeeli, A. H. O. Al Mansor, M. Andreevich, Application of M5 algorithm of decision tree in simulation and investigation of effective factors of erosion in rangelands and forests, *Caspian Journal of Environmental Sciences*, 2023, **21**, 533-541, doi: 10.22124/cjes.2023.6929.
[76] R. Hecht-Nielsen, Kolmogorov's mapping neural network existence theorem. Reference IEEE Press New York, 1987.
[77] Hush, Classification with neural networks: a performance analysis, IEEE 1989 International Conference on Systems Engineering. Fairborn, OH, USA. IEEE, 1989, 277-280, doi: 10.1109/ICSYSE.1989.48672.
[78] B. Ripley, Statistical Aspects of Neural Networks; Barndorff-Nielsen, O.E., Jensen, J.L., Kendall, W.S., Eds.; Networks and Chaos–Statistical and Probabilistic Aspects. In.: Chapman and Hall: London, UK (1993).
[79] J. Paola. Neural network classification of multispectral imagery, MSc thesis, The University of Arizona, USA.1994.
[80] C. Wang, A theory of generalization in learning machines with neural network applications. Ph.D. Thesis, University of

Pennsylvania. 1994.
[81] D. Abdullah, K. Gartsiyanova, K. Mansur qizi, E. A. Javlievich, M. B. Bulturbayevich, G. Zokirova, M. N. Nordin, An artificial neural networks approach and hybrid method with wavelet transform to investigate the quality of Tallo River, Indonesia, *Caspian Journal of Environmental Sciences*, 2023, **21**, 647-656, doi: 10.22124/cjes.2023.6942.
[82] Y. Ansari, A. Hashemi, Neural network approach in assessment of fiber concrete impact strength, *Journal of Civil Engineering and Materials Application*, 2017, **1**, 88-97, doi: 10.15412.12010301
[83] M. Fallah, Z. Pirali Zefrehei, S.A. Hedayati, T. Bagheri, Comparison of temporal and spatial patterns of water quality parameters in Anzali Wetland (southwest of the Caspian Sea) using Support vector machine model, *Caspian Journal of Environmental Sciences*, 2021, **19**, 95-104, doi:10.22124/CJES.2021.4500.
[84] I. Rustamovich Sultanbekov, I. Yurievna Myshkina, L. Yurievna Gruditsyna. Development of an application for creation and learning of neural networks to utilize in environmental sciences, *Caspian Journal of Environmental Sciences*, 2020, **18**, 595-601, doi: 10.22124/CJES.2020.4491.
[85] S. Alzabeebee, Explicit soft computing model to predict the undrained bearing capacity of footing resting on aggregate pier reinforced cohesive ground, *Innovative Infrastructure Solutions*, 2021, **7**, 105, doi: 10.1007/s41062-021-00706-7.

